To the Graduate Council:

I am submitting herewith a thesis written by David H. Plemmons entitled "Electron Density and Temperature Determination of a Laser-Induced Plasma in Hydrogen Gas." I have examined the final copy of this thesis for form and content and recommend that it be accepted in partial fulfillment of the requirements for the degree of Masters of Science, with a major in Physics.

J. W. L. Lewis, Major Professor

We have read this thesis
and recommend its acceptance:

Accepted for the Council:

Associate Vice Chancellor
and Dean of The Graduate School

STATEMENT OF PERMISSION TO USE

In presenting this thesis in partial fulfillment of the requirements for a Master's degree at The University of Tennessee, Knoxville, I agree that the Library shall make it available to borrowers under rules of the Library. Brief quotations from this thesis are allowable without special permission, provided that accurate acknowledgment of the source is made.

Permission for extensive quotation from or reproduction of this thesis may be granted by my major professor, or in his absence, by the Head of Interlibrary Services when, in the opinion of either, the proposed use of the material is for scholarly purposes. Any copying or use of the material in this thesis for financial gain shall not be allowed without my written permission.

Signature David Plemmons

Date 1-6-94

Electron Density and Temperature Determination of a Laser-Induced Plasma in Hydrogen Gas

A Thesis

Presented for the

Master of Science

Degree

The University of Tennessee, Knoxville

David H. Plemmons

May 1994

Dedications

This thesis is dedicated to my wife Sharon Dale Chaffin Plemmons without whose encouragement and support this thesis would not have been possible.

Acknowledgements

I would like to take this opportunity to thank the faculty and staff of the CLA for their assistance in the completion of this thesis. I would especially like to thank Dr. Christian Parigger who worked with me on a daily basis on the conception and implementation of the experiments and on the analysis of the data. I am equally grateful for Dr. J. W. L. Lewis' insightful comments and suggestions on both the theoretical and experimental aspects of this thesis. I would also like to thank Newton Write, Fred Schwartz and Bruce Hill for their assistance and suggestions.

Many computer programs were used in the acquisition and analysis of data. I would like to thank Dr. Parigger for the use of his data acquisition and analysis programs. I also thank Jim Hornkohl for his interactive plot program used extensively in data analysis.

Abstract

In dense plasmas that contain hydrogen, electron number densities can be determined from the measured full widths at half maximum of the Balmer lines. Electron temperatures can be inferred from Boltzmann plots of the Balmer series. These techniques are applied to characterize the temporal evolution of the electron number density and temperature of a plasma generated by a pulsed laser in pure hydrogen gas. The excitation source is a pulsed Nd:YAG laser which has a wavelength of 1.064 μm and a temporal pulse width of 7.5 ns. The average energy per pulse is 150 mJ.

Using time resolved spectroscopy, electron number densities in the range of 10^{16} to 10^{19} cm^{-3} are inferred for the first few microseconds of the plasma decay. The corresponding temperatures range from approximately 5,000 K to 15,000 K. The time resolution of these results is 6 ns for the electron temperatures and 2 to 100 ns for the electron number densities.

Contents

List of Figures

List of Tables

1 INTRODUCTION

Laser-induced breakdown in gases occurs when a laser beam is focused to a sufficiently small diameter that the power density is enough to ionize the gas molecules in the focal volume. This phenomenon is also referred to in the literature as optical breakdown, optical discharge, laser spark, laser-induced plasma, or laser-induced microplasma and other names descriptive of the phenomena.

Laser-induced breakdown in gas is achieved as follows. Initially, electrons are stripped from gas molecules through multi-photon absorption. The free electrons are accelerated through inverse bremsstrahlung. The accelerated electrons collide with gas molecules causing further ionization. This process continues resulting in a hot dense plasma in the region of the focal volume. Although optical breakdown can be achieved with powerful continuous wave lasers, only pulsed laser-induced breakdown will be considered here.

The minimum power density required for breakdown is defined to as the threshold. The threshold value is a function of gas species and pressure and laser wavelength and pulse-width. The breakdown threshold of clean laboratory air at atmospheric pressure with a laser wavelength of 1.06 μm and a pulse width of 10 ns is approximately 80 GW/cm^2 [1].

Associated with the formation of the plasma by a pulsed laser is a shock wave. This shock wave is noticeable, for power densities well above threshold, in that there is a loud pop that accompanies the bright flash of light that is emitted by the laser

spark.

Initially, after formation of the plasma, there is a strong continuum of free-electron radiation. As the plasma begins to expand and cool, electron-ion recombination processes become more prominent. Ionic and atomic lines begin to emerge from the continuum. While excited atoms and ions decay to lower states, the emitted radiation may be observed and used to characterize the plasma. As the plasma cools further, molecular recombination occurs, and excited molecules are formed. These molecules radiate, and this radiation can also be used to characterize the plasma. For example, J. O. Hornkohl et al [2] recently reported vibrational-rotational temperatures inferred from the comparison of calculated and experimental diatomic spectra emitted from a laser-induced plasma.

Laser-induced breakdown was first observed in atmospheric air with a Q-switched ruby laser [3]. Subsequently, optical breakdown has been studied in a variety of gases as well as in aerosols and liquids, and on the surfaces of solids. Much effort has been expended in characterizing the plasma generated by a laser spark and in applying this phenomenon to spectrochemical analysis. This area of research is commonly referred to as laser-induced breakdown spectroscopy or LIBS. The primary advantage of LIBS is that it can be applied to any system that allows optical access. This freedom makes accessible corrosive, high temperature, or otherwise hostile and inaccessible systems. This thesis is not concerned with spectrochemical analysis but rather with the characterization of the plasma generated by a pulsed laser. In particular we will

determine the electron number density and temperature of such a plasma.

In laser-induced optical breakdown plasmas atomic lines are frequently selected to characterize electron number density and temperature. For typical plasma conditions, Stark broadening of atomic lines is particularly useful for determining electron number densities, and Boltzmann plots are a standard tool for electron temperature determination.

The Stark effect in general broadens line shapes of atomic species and results from the splitting of electronic energy levels in an electric field. One-electron atoms exhibit the linear Stark effect which causes a symmetrical splitting of the energy levels proportional to the strength of the electric field. Multielectron atoms do not exhibit this linear effect, but are subject in second order to the quadratic Stark effect. The quadratic effect results in an asymmetrical splitting of the energy levels, the magnitude of which is much smaller than the linear effect. Reference [4] gives a good discussion of the linear and quadratic Stark effects. One-electron atoms are also subject to the quadratic effect in second order, but the resulting line broadening is much smaller than that for the linear effect. Therefore, hydrogenic species have a much broader line width than multielectron species for any applied electric field.

In plasmas the free charges produce an electric field that is a function of the electron density in the plasma. Thus, the theoretical treatment of the Stark effect may be applied to the line widths of atomic lines emitted from the plasma to determine the electron density in the plasma.

The broader line widths make hydrogenic species particular useful for electron density determination. It is therefore advantageous to have hydrogenic species in the sample. Frequently hydrogen exists as a constituent part of the sample and can readily be used in diagnostics [5, 6, 7, 8]. Alternatively, hydrogen may be introduced in small amounts as a diagnostic probe [9, 10].

Boltzmann plots are extensively used in atomic and molecular spectroscopy. Applications can be found throughout the literature [2, 5, 8]. This technique is based upon the relative intensities of the radiation emitted as electrons decay from various excited states to a common lower state. The hydrogen Balmer series is the series of lines which are emitted as the excited electron decays to the n = 2 energy level of the hydrogen atom and, as such, is well suited for this purpose.

In this thesis, for a decaying plasma generated in hydrogen gas by a focused laser pulse, we characterize the electron density and temperature using the Stark broadened H_α and H_β lines for electron density and Boltzmann plots of the Balmer series for electron temperature. For electron densities from about 10^{15} cm^{-3} to 3×10^{17} cm^{-3} the H_β line is typically used as an accurate density diagnostic [11]. At higher densities it is desirable to use the H_α line for several reasons. The H_β line becomes very wide, and the asymmetry that is present between the red and blue peaks becomes more pronounced. In addition, the wings of the H_γ, H_δ, etc. lines superimpose the H_β line and causes further difficulties in determining the line width. Conversely, the H_α line is not as wide as the H_β for a given electron density and is more remote from other

lines of the series. Thus, the H_α line suffers less from distortion due to superposition of the wings of the other lines.

2 PREVIOUS WORK

Theoretical and experimental work on Stark broadening of atomic lines in plasmas is well documented in the literature. A valuable reference on this subject is a book written by Hans Griem–*Spectral Line Broadening by Plasmas* [11]. In his book Griem discusses extensively the physical mechanisms by which atomic lines are broadened in plasmas. He presents tabulated Stark-broadened profiles of hydrogen lines for the Lyman and Balmer series for various plasma conditions. He also presents theoretical results for ionized helium and numerous multielectron atoms and ions.

There are, however, some refinements that have been made to the theory since the publication of this book. In particular, D. H. Oza et al [12] have calculated additional collisional broadening effects for the H_α line that are significant for electron densities less than 10^{17} cm^{-3}.

Much of the experimental work has been done on steady-state plasma sources such as electrical arcs [13]. Most of this work was done for the purpose of verification of theoretical predictions. We are interested in plasmas produced by pulsed lasers, and, in particular, the characterization of such a plasma using atomic hydrogen emission lines. In the following paragraphs we summarize some of the experimental results that pertain specifically to this topic.

Optical breakdown in hydrogen gas was previously studied by Litvak and Edwards [14] in 1966. A pulsed ruby laser (694 nm, 30 ns pulse width and 200 mJ/pulse) was used to create optical breakdown in hydrogen gas from 1 to 70 atmospheres. Using

the Stark broadened H_α line, electron densities up to 4×10^{18} cm^{-3} were reported for atmospheric hydrogen gas. Electron temperature up to 20,000 K were determined using line-to-continuum ratios.

T. P. Evtushenko et al [15] performed time-resolved spectroscopic studies of a Q-switched ruby laser spark (0.5 to 1 J/pulse, 30 to 40 ns pulse width) in helium gas which contained traces of hydrogen. They inferred from H_α and He I 5876 Å line widths electron densities of 5 to 7 $\times 10^{18}$ cm^{-3} at early stages of the spark development. They also reported on the observation of the plasma decay going through two stages. "In the first stage ($\sim$ 100 ns), the plasma exhibited a high electron temperature and density while emitting an intense spectral continuum and heavily broadened lines of neutral and ionized atoms. The second stage involves a gradual cooling off of the plasma, and only lines of neutrals are emitted in this stage. This stage last some tens of microseconds." We have observed the same type of behavior is observed in the pure hydrogen plasma except, of course, for the presence of ion lines.

Eickmans et al [8] applied LIBS to optical breakdown in micrometer-size water droplets. The excitation source used was a frequency doubled (532 nm), Nd:YAG, 20 ns laser pulse with a focused power density of approximately 28 GW/cm^2. They used H_α and H_β line widths to measure electron densities in the range of 10^{18} cm^{-3}. H_α and H_β two-line Boltzmann plots were used to obtain electron temperatures. They reported electron temperatures of approximately 5000 K with estimated uncertainties of about 50%.

J. Uhlenbusch and W. Viöl [16] studied the effects of pulsed optical discharge in a gaseous hydrogen environment for pressures of 10 to 55 atmospheres. For these studies they used a 200 ns CO_2 laser pulse with an average power of 1 kW per pulse. Using H_β line widths they reported a maximum electron density (at the end of the laser pulse) of $\sim 3\times10^{18}$ cm^{-3} for the 10 atmosphere case. H_β line-to-continuum ratios yielded maximum electron temperatures of $\sim$ 40,000 K, again for the 10 atmosphere case. For higher pressures–and, therefore, higher electron densities–they were unable to give reliable numbers for electron density and temperature due to the excessive broadening of the H_β line.

In there work Uhlenbusch and Viöl compared the measured spectral distance between the red and blue peak of the H_β line as a function of the full width at half maximum (FWHM). The results for the wavelength separation of the two maxima agreed with the theory to within a factor of two.

A more recent experiment that encompasses these ideas is one performed by Josef Simeonsson and Andrzej Miziolek [5]. They used a pulsed ArF Excimer 193 nm laser with 10 mJ of energy in a 10 ns pulse to create microplasmas in various gases. They employed H_α line width plasma diagnostic techniques on breakdown in gaseous methanol flowing at 150 cm^3/min to find electron densities in the range of 10^{17} cm^{-3} to 10^{18} cm^{-3}. They found excitation temperatures of 15,000 K to 20,000 K from Boltzmann plots of the 777 nm and 795 nm neutral oxygen emission lines.

The Simeonsson experiment, published in 1993, illustrates that atomic hydrogen

emission lines are still of present day interest. Even though they offer no refinements to the theory of Stark broadening, they use the existing theory to infer the plasma conditions under study. Such use of Stark-broadened atomic lines is a standard tool in plasma diagnostics.

As mentioned in the introduction, Boltzmann plots are also standard fare in plasma diagnostics. However, there appears to be a lack of published Boltzmann plot results for the hydrogen Balmer series. This may be due in part to the broad spectral range spanned by the Balmer series. The H_α line lies at 6562.8 Å and the series limit is at 3645.6 Å.

This thesis presents the methodology for the determination of electron density and temperature in a dense plasma created by a pulsed Nd:YAG laser. We are interested primarily in establishing a procedure by which these parameters can be determined from the individual, time-resolved, experimental data [17, 18].

In the following chapter, Chapter 3, we present an overview of the theoretical foundation of Stark broadening and Boltzmann plots. Chapters 4 and 5 discuss the experimental requirements and physical setup. In Chapter 6 the techniques used in data analysis are introduced and the results are presented and discussed. Chapter 7 gives the preliminary results of an additional two dimensional experiment performed separately from those described in Chapter 5. In Chapter 8 we give a summary of the analysis techniques and results and discuss of the utility of these methods to future projects of interest to our group.

3 THEORY

3.1 Line Broadening

The observed line width of an atomic line emitted from a plasma is the convolution of Doppler, pressure (Stark, Van der Waals and resonance), natural and instrumental profiles [19]. The dominant mechanisms by which atomic lines are broadened in a plasma are Doppler broadening and Stark broadening. Doppler-broadened lines are Gaussian. Stark-broadened profiles are Lorentzian near the line center with Holtzmark wings.

Doppler broadening is due to the motion of the emitting atoms relative to the observer. For a gas in thermodynamic equilibrium at a temperature T in a closed cell the resulting Boltzmann velocity distribution leads to a Doppler width

$$\delta\lambda_D = \frac{2}{c}\sqrt{\frac{2RTln2}{M}}\lambda_0 = 7.16 \times 10^{-7}\sqrt{\frac{T}{M}}\lambda_0, \qquad (1)$$

where M is the mass number of the emitting atom. At a temperature of 10^4 K the Doppler width of the H_α line is $\sim$ 0.5 Å.

Stark broadening is due to the interaction between an emitting atom and charged particles within the plasma. The interaction of the atom with the electric field resulting from the charged particles is described by the Stark effect. For one electron atoms or ions the dominant term is the linear Stark effect, which is proportional to the magnitude of the electric field. The linear effect results in a symmetrical splitting of the atomic energy levels and thus leads to a symmetrically broadened, unshifted, unresolved, atomic spectral line. The FWHM of hydrogenic lines is given, to a first

approximation, by the relation [20]

$$\delta\lambda_S = C(N_e, T)N_e^{2/3} \tag{2}$$

where C depends only weakly on temperature. This relation is used if a temperature independent treatment is applied. If electron temperatures are known the relation

$$\delta\lambda_S = 2.507 \times 10^{-10} a(T)N_e^{2/3} \tag{3}$$

can be used to infer electron density from line width data. The Stark parameter a for the hydrogen Balmer lines is available over a wide range of electron densities and temperatures. Reference [11]. has tabulated values of the Stark parameter for electron temperatures from 5,000 to 40,000 K and electron densities from 10^{15} to 10^{19} cm^{-3} for the H_α line and from 10^{14} to 10^{18} cm^{-3} for the H_β line.

The linear Stark effect of excited one-electron atoms is such that the resulting line broadening increases with the atomic excitation energy. Thus, at a given electron density, the H_β is broader than the H_α line; the H_γ line is broader than the H_β line, and so on to the series limit.

The theory of linear Stark-broadening of hydrogen emission lines predicts symmetrically broadened, unshifted, profiles. Figures 1 and 2 show theoretical H_α and H_β profiles according to Ref. [11]. Typical experimental H_α and H_β profiles monitored during the course of this thesis are shown in Figs. 3 and 4. While the experimental H_α lines appear to be symmetric, the experimental H_β lines are clearly asymmetric at early times in the plasma decay. The asymmetry is more pronounced at higher

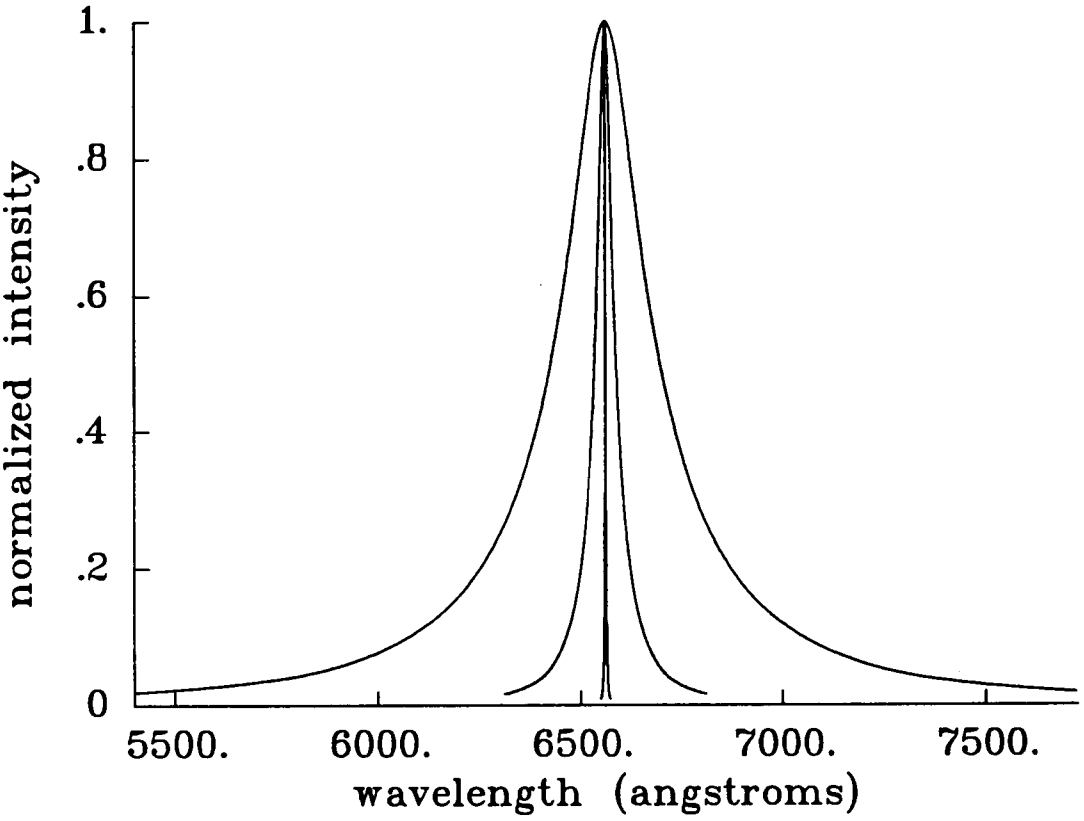

Figure 1: Theoretical H_α profiles for electron densities of 10^{16}, 10^{17}, and 10^{19} cm^{-3}

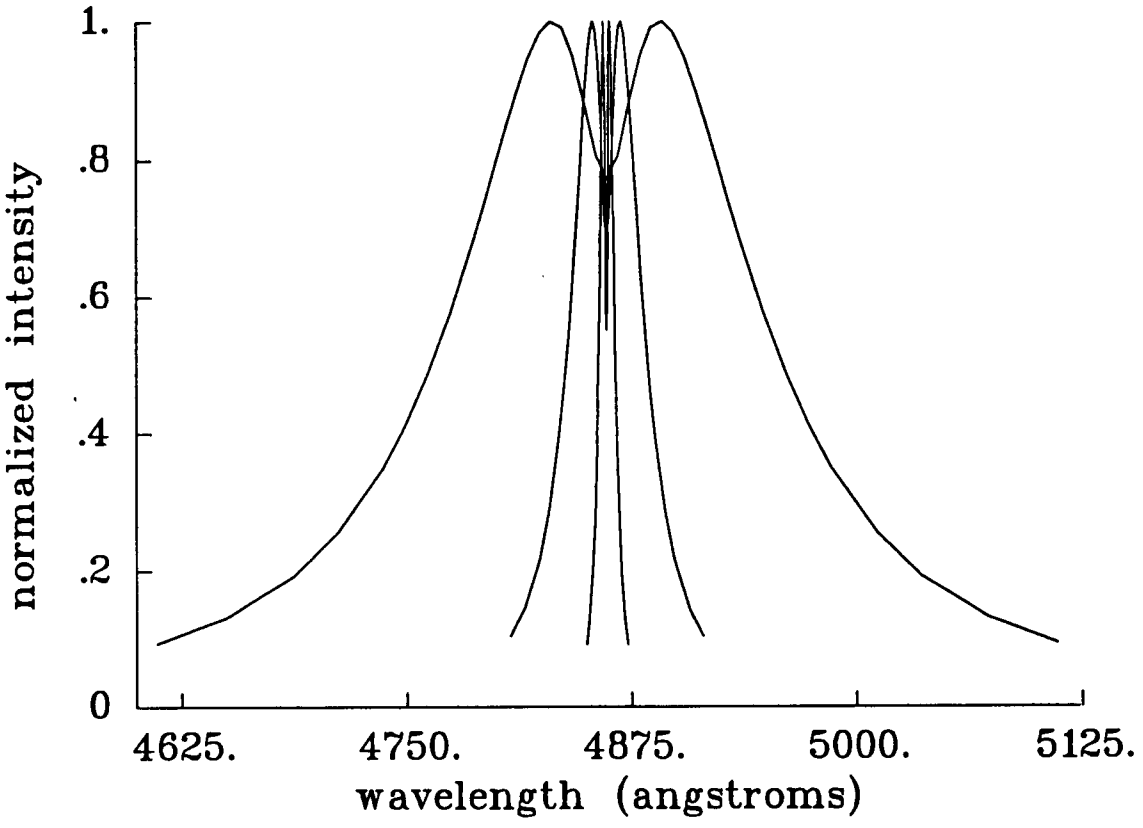

Figure 2: Theoretical H_β profiles for electron densities of 10^{16}, 10^{17}, and 10^{18} cm^{-3}

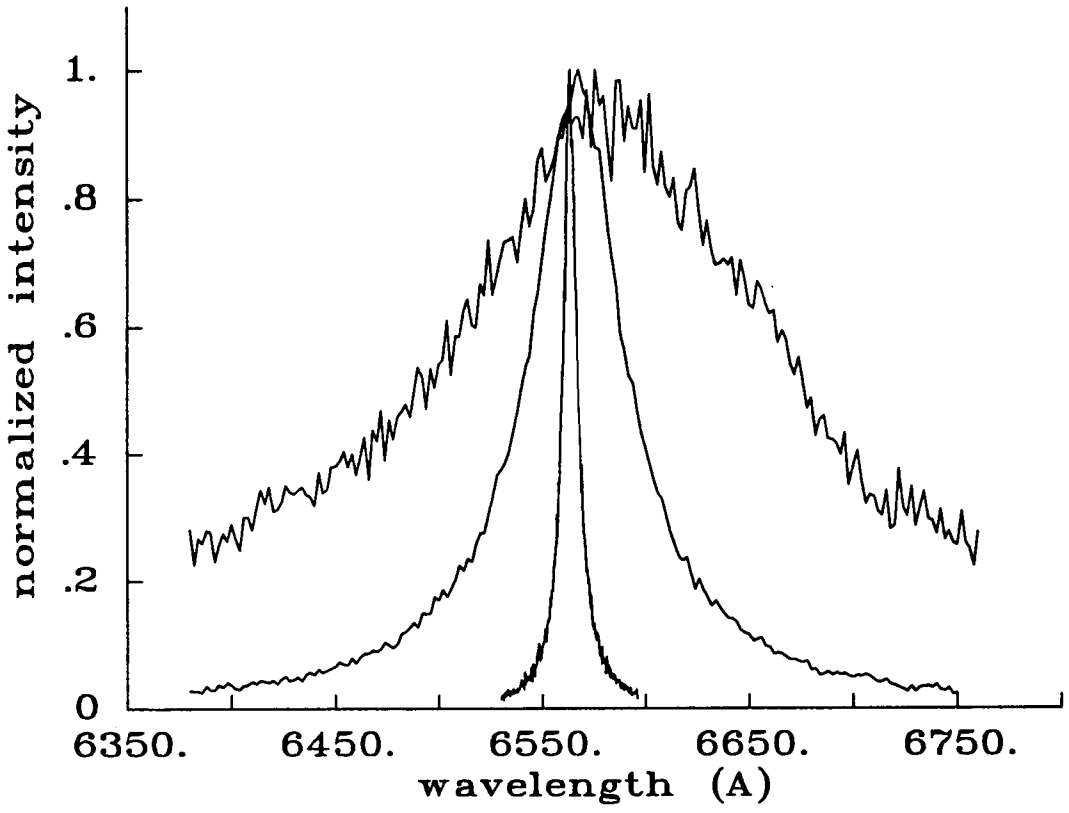

Figure 3: Experimental H_α profiles for electron densities of 7.1×10^{16}, 1×10^{18} and 5.4×10^{18} cm^{-3}

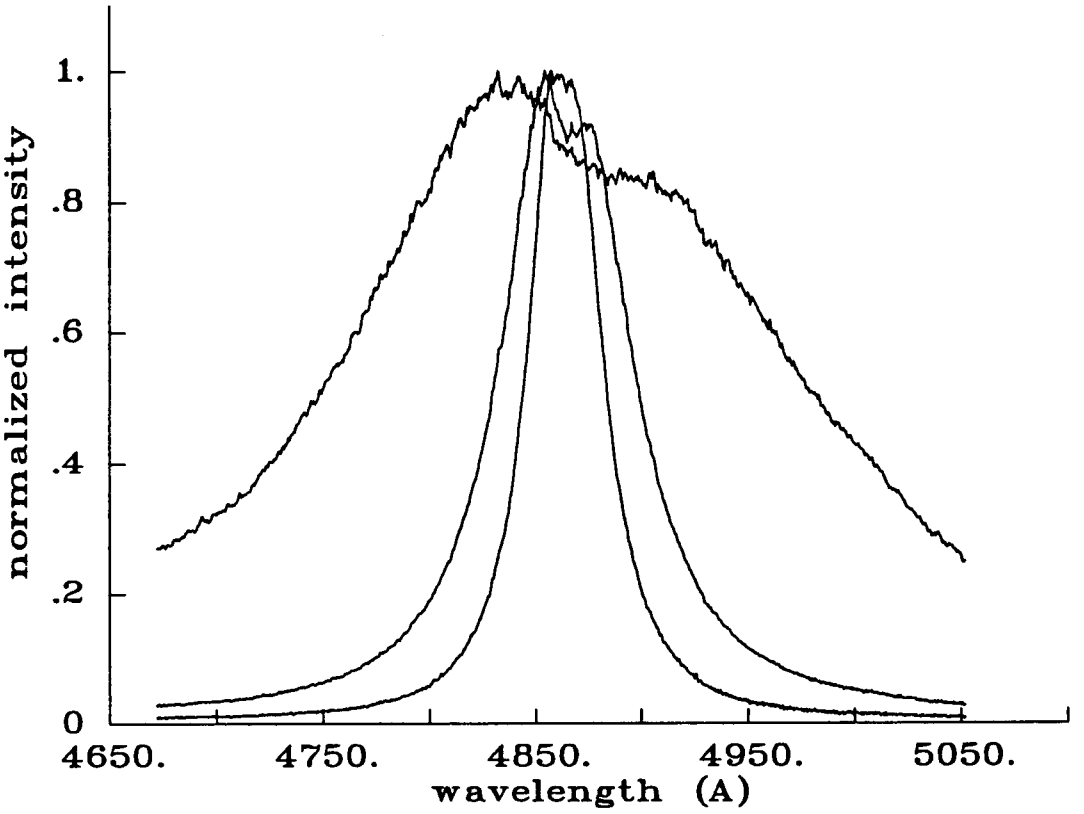

Figure 4: Experimental H_β profiles for electron densities of 7.6×10^{16}, 2×10^{17} and 1×10^{18} cm^{-3}

electron densities and is attributed to quadratic effects [16]. It is this effect, along with the width of the profile, which makes the H_β ill-suited for density determination at high electron number densities. Note also that the H_α line is red shifted from its neutral position. This shift is also due to quadratic effects [21].

3.2 Boltzmann Plots

Boltzmann plots are used to determine the population or excitation temperature of the emitting species from the relative intensities of a series of emission lines. The absolute intensity of radiation emitted by an atom as an electron decays spontaneously from a state 2 to a state 1 can be written as

$$I_{21} = const\ g_2 A_{21} \nu_{12} e^{-E_2/kT} \tag{4}$$

where g_2 is the degeneracy or statistical weight of level 2, A_{21} is the Einstein coefficient of spontaneous emission, ν_{12} is the frequency of emitted radiation, E_2 is the energy of level 2, k is the Boltzmann constant and T is the excitation temperature.

If the gas sample is in thermodynamic equilibrium or local thermodynamic equilibrium (LTE), then the excited states are populated and depopulated primarily through collisional processes. Under such conditions the excitation temperature can be equated with the mean kinetic energy of the colliding particles, 3/2 kT. Since electrons are much more efficient than atoms, molecules or ions in collisional excitation and deexcitation processes, the excitation temperature under LTE is referred to as the electron temperature.

One advantageous aspect of Boltzmann plots is that only relative intensity measures are required; i.e., we need not concern ourselves with the constant that multiplies the term on the right of Eq. (4). Rewriting Eq. (4) using $\nu_{12} = c/\lambda_{12}$ we have

$$ln\left(\frac{I_{21}\lambda_{12}}{g_2 A_{21}}\right) = ln(c \cdot const) - \frac{E_2}{kT} \tag{5}$$

If we plot $ln\left(\frac{I_{21}\lambda_{12}}{g_2 A_{21}}\right)$ versus $\frac{E_2}{k}$ then we have a straight line, the negative slope of which is equal to $1/T$.

3.3 Validity of the LTE Assumption

Before we can use Boltzmann plots to infer electron temperatures, we must be sure that the plasma is in either thermodynamic equilibrium or local thermodynamic equilibrium. The LTE assumption is valid if atoms (or molecules) in the plasma have a higher probability of excitation and de-excitation by collisions than by radiative processes. That is, collisional processes dominate radiative processes. This effectively requires a minimum electron density. The minimum electron density required for LTE between two states is given by [20]

$$N_e \gg 1.6 \times 10^{12}\sqrt{T}(\Delta E)^3 \text{cm}^{-3} \tag{6}$$

where T is the electron temperature and ΔE is the energy difference between the two states. For the Balmer series we have $\Delta E_{H_\alpha} = 1.88$ eV, $\Delta E_{H_\beta} = 2.54$ eV, $\Delta E_{H_\gamma} = 3.01$ eV, and for the series limit $\Delta E = 3.4$ eV.

For $\Delta E = 3.4$ eV and $T = 15{,}000$ K, $N_e \gg 7.7 \times 10^{15}$ cm^{-3}. For $\Delta E = 3.4$ eV and $T = 8000$ K, $N_e \gg 5.6 \times 10^{15}$ cm^{-3}. The plasma conditions studied herein are

well within this range.

The relaxation time of the plasma to LTE for our experimental conditions is on the order of 1 ns [5]. This relaxation time is shorter by a factor of 2 than the minimum gate width used in this experiment.

4 EXPERIMENTAL REQUIREMENTS

In the course of studying laser-induced breakdown in a liquid droplet we observed hydrogen Balmer lines in the visible portion of the spectrum during a broad spectral scan of the plasma emission. It was recognized that these lines could yield quantitative information about the plasma. We needed a technique by which we could determine electron density and temperature at early times in the plasma decay. We also recognized that the theory of Stark broadening of atomic lines and Boltzmann plots could be utilized for such an evaluation.

As mentioned in the introduction, it is desirable to use H_β line profiles for density determination for moderately high electron number densities since the H_β line typically yields a more accurate electron number density [11]. However, the H_β line was superimposed with a C_2 Swan band in the original plasma, and quantitative interpretation of the data was difficult. In addition, the electron densities of the laser-induced plasma are so high at early times that the H_β line cannot be used. In the droplet plasma the H_α line was relatively clean. It was decided that the electron density inference would best be performed with the H_α line. The following experiments were conducted in pure hydrogen gas so that the Balmer lines could be examined without the complication of impurities and so that Boltzmann plots of sufficiently large signal levels could be obtained.

5 EXPERIMENTAL ARRANGEMENT

A Continuum YG680S-10 Nd:YAG laser operated at 1.064 μm and 10 Hz is used to generate the plasma. The energy output of the laser is 150 mJ/pulse with a 7.5 ns pulse width. The output beam is focused with a 10 cm focal length lens into a gas cell that contains research-grade hydrogen gas where optical breakdown occurs.

The power density of the focused laser pulse is well in excess of the breakdown threshold. The resulting laser spark, when viewed with the eye is about 1 centimeter long, 1 or 2 millimeters wide and has internal structure. The reader is referred to Appendix A for a further description of the laser spark.

The gas sample is prepared by first evacuating the cell with a diffusion pump. The cell is then filled with research grade hydrogen gas to the desired pressure. The gas filling is monitored using a gauge mounted directly to the cell. The precision of the gauge is $\pm$ 25 torr.

The plasma emission is imaged one-to-one onto the spectrometer slit using the appropriate optical arrangement. Figure 5 shows the schematic of the experimental arrangement. Figure 6 shows the two optical arrangements used in this thesis. The spectrometer is oriented such that the slit is perpendicular to the direction of the laser beam. Thus we are viewing the breakdown perpendicular to the Rayleigh range of the focused radiation.

The experiment is externally synchronized to 10 Hz through delay generators. The laser is controlled externally where the delay generators are used to charge, fire,

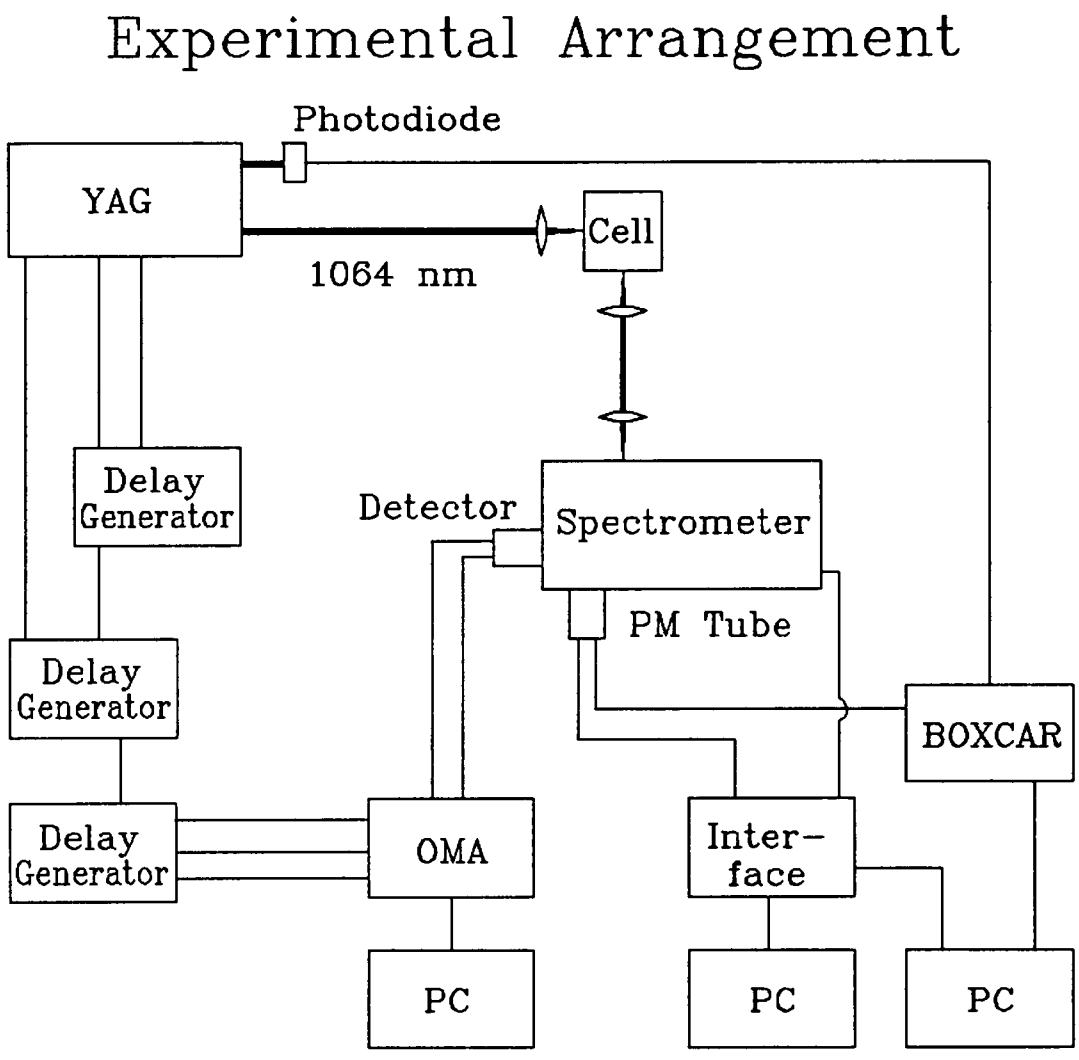

Figure 5: Schematic of the experimental arrangement

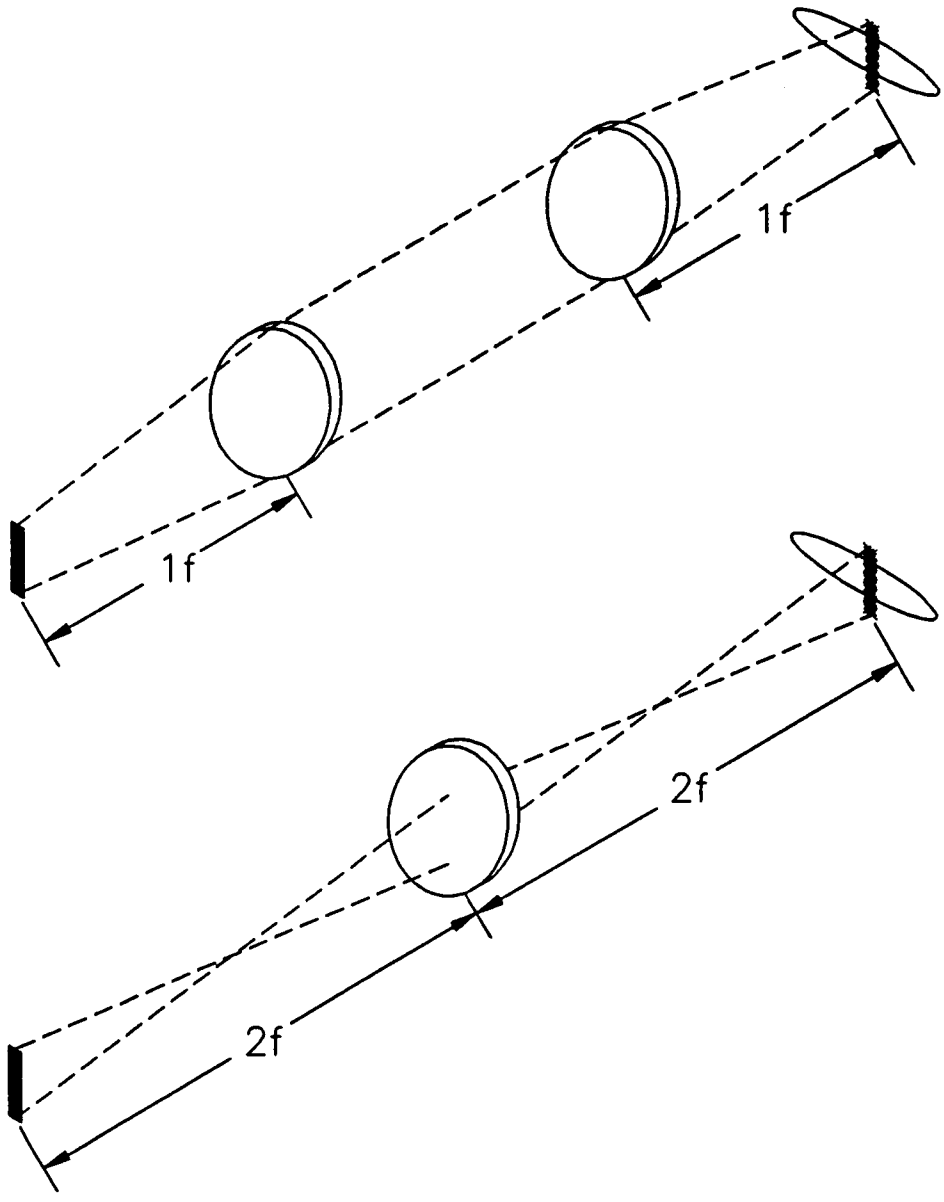

Figure 6: Projection of the spectrometer slit onto the plasma

and Q-switch. Detector gating and delay are referenced to the laser pulse through the delay generators or by use of an optical trigger. In all cases the timing jitter of the gate is less than 2 ns.

Two monochromators are used to disperse the plasma emission. Whenever possible we utilize the Optical Multichannel Analyzer (OMA) together with a linear photodiode array to record the spectra. This is the preferred method since it allows us to capture an entire profile in a single shot. We find this procedure adequate for recording a narrow spectral band at high resolution and broad spectral band at low resolution. For lines of spectral width less than three hundred angstroms, high-resolution data can be obtained using this arrangement. The OMA also is also used for recording the entire Balmer series at low resolution.

Early in the plasma decay the hydrogen lines are too broad to measure with the linear photodiode array and maintain optimum resolution. Therefore, at early times, we use a photomultiplier tube and scan the spectrometer over the spectral range of interest. In this fashion we are able to maintain optimum resolution and record more complete line profiles. This technique works well provided that the optical breakdown is repeatable and stable over a period of time. It typically takes from thirty minutes to one hour to record a single line. In addition to the broad spectral range that can be covered with this technique, the BOXCAR gated integrator also provides a shorter gate width than is available with the OMA.

The linear photodiode array detector we use is gated. The gate width is variable

Table 1: Experimental apparatus

A. Laser	
laser	Continuum YG680S Nd:YAG
wavelength	1.064 μ
repetition rate	10 Hz
pulse width	7.5 ns
energy/pulse	150 mJ
B. Detection System I	
1. spectrometer	Jobin Yvon 0.64 Czerny-Turner
grating	3600 g/mm
slit width	20 μm
2. detector	Photomultiplier tube: RCA C41034A
3. signal processing	BOXCAR: EG&G Model 4402 plus 4422 gated integrator
4. temporal resolution	$\geq$ 2 ns
5. spectral resolution	0.2 Å
C. Detection System II	
1. spectrometer	Jarrell Ash 1/4 m crossed Czerny Turner
gratings	150 or 1800 g/mm
slit width	200 μm
2. detector	EG&G intensified/gated (1×1024) linear photodiode array
3. signal processing	EG&G optical multi-channel analyzer (OMA)
4. temporal resolution	$\geq$ 6 ns
5. spectral resolution	40 Å (150 g/mm), 2.5 Å (1800 g/mm)

from 6 ns to 10 ms, and the gate delay is "continuously" variable. For the photomultiplier tube, gate width and delay are controlled and through a BOXCAR signal integrator. The minimum gate width used with the BOXCAR is 2 ns. The equipment used in this experiment is listed in Table 1.

Using either the BOXCAR or the OMA with the appropriate spectrometer and detector, we record hydrogen lines emitted from the plasma at various delays. The data files that have been recorded and analyzed are listed in Table 2.

Table 2: Experimental data

time delay (μs)	gate width (ns)	cell pressure (torr)	spectrometer - detector (grating)	spectrum
0.005	2	810	JY - BOXCAR	H_α
0.020	2	810	JY - BOXCAR	H_α
0.040	2	810	JY - BOXCAR	H_α
0.060	2	810	JY - BOXCAR	H_α
0.080	2	810	JY - BOXCAR	H_α
0.100	20	810	JY - BOXCAR	H_α
0.450	100	810	JY - BOXCAR	H_α
1.0	100	810	JY - BOXCAR	H_α
2.0	100	810	JY - BOXCAR	H_α
4.0	100	810	JY - BOXCAR	H_α
0.030	100	810	JA - OMA (1800 g/mm)	H_α
0.050	100	810	JA - OMA (1800 g/mm)	H_α
0.200	100	810	JA - OMA (1800 g/mm)	H_α
0.300	100	810	JA - OMA (1800 g/mm)	H_α
0.400	100	810	JA - OMA (1800 g/mm)	H_α
0.500	100	810	JA - OMA (1800 g/mm)	H_α
0.600	100	810	JA - OMA (1800 g/mm)	H_α
0.700	100	810	JA - OMA (1800 g/mm)	H_α
0.800	100	810	JA - OMA (1800 g/mm)	H_α
0.900	100	810	JA - OMA (1800 g/mm)	H_α
1.0	100	810	JA - OMA (1800 g/mm)	H_α
1.2	100	810	JA - OMA (1800 g/mm)	H_α
1.4	100	810	JA - OMA (1800 g/mm)	H_α
1.6	100	810	JA - OMA (1800 g/mm)	H_α
1.9	100	810	JA - OMA (1800 g/mm)	H_α
2.5	100	810	JA - OMA (1800 g/mm)	H_α
3.0	100	810	JA - OMA (1800 g/mm)	H_α
0.0	6	810 & 1010	JA - OMA (150 g/mm)	Balmer Series
0.05	6	810 & 1010	JA - OMA (150 g/mm)	Balmer Series
0.10	6	810 & 1010	JA - OMA (150 g/mm)	Balmer Series
0.15	6	810 & 1010	JA - OMA (150 g/mm)	Balmer Series
0.20	6	810 & 1010	JA - OMA (150 g/mm)	Balmer Series
0.25	6	810 & 1010	JA - OMA (150 g/mm)	Balmer Series
0.30	6	810 & 1010	JA - OMA (150 g/mm)	Balmer Series
0.35	6	810 & 1010	JA - OMA (150 g/mm)	Balmer Series
0.40	6	810 & 1010	JA - OMA (150 g/mm)	Balmer Series
0.45	6	810 & 1010	JA - OMA (150 g/mm)	Balmer Series

Table 2. (continued)

time delay (μs)	gate width (ns)	cell pressure (torr)	spectrometer - detector (grating)	spectrum
0.50	6	810 & 1010	JA - OMA (150 g/mm)	Balmer Series
0.55	6	810 & 1010	JA - OMA (150 g/mm)	Balmer Series
0.60	6	810 & 1010	JA - OMA (150 g/mm)	Balmer Series
0.65	6	810 & 1010	JA - OMA (150 g/mm)	Balmer Series
0.75	6	810 & 1010	JA - OMA (150 g/mm)	Balmer Series
0.80	6	810 & 1010	JA - OMA (150 g/mm)	Balmer Series
1.0	6	810 & 1010	JA - OMA (150 g/mm)	Balmer Series
1.2	6	810 & 1010	JA - OMA (150 g/mm)	Balmer Series
1.4	6	810 & 1010	JA - OMA (150 g/mm)	Balmer Series
1.6	6	810 & 1010	JA - OMA (150 g/mm)	Balmer Series
2.0	6	810 & 1010	JA - OMA (150 g/mm)	Balmer Series
2.5	6	810 & 1010	JA - OMA (150 g/mm)	Balmer Series
3.0	6	810 & 1010	JA - OMA (150 g/mm)	Balmer Series
0	6	810 & 1010	JA - OMA (1800 g/mm)	H_β
0.100	6	810 & 1010	JA - OMA (1800 g/mm)	H_β
0.200	6	810 & 1010	JA - OMA (1800 g/mm)	H_β
0.300	6	810 & 1010	JA - OMA (1800 g/mm)	H_β
0.400	6	810 & 1010	JA - OMA (1800 g/mm)	H_β
0.500	6	810 & 1010	JA - OMA (1800 g/mm)	H_β
0.600	6	810 & 1010	JA - OMA (1800 g/mm)	H_β
0.700	6	810 & 1010	JA - OMA (1800 g/mm)	H_β
0.800	6	810 & 1010	JA - OMA (1800 g/mm)	H_β
0.900	6	810 & 1010	JA - OMA (1800 g/mm)	H_β
1.0	6	810 & 1010	JA - OMA (1800 g/mm)	H_β
1.1	6	810 & 1010	JA - OMA (1800 g/mm)	H_β
1.2	6	810 & 1010	JA - OMA (1800 g/mm)	H_β
1.4	6	810 & 1010	JA - OMA (1800 g/mm)	H_β
1.6	6	810 & 1010	JA - OMA (1800 g/mm)	H_β
1.8	6	810 & 1010	JA - OMA (1800 g/mm)	H_β
2.0	6	810 & 1010	JA - OMA (1800 g/mm)	H_β
2.5	6	810 & 1010	JA - OMA (1800 g/mm)	H_β
3.0	6	810 & 1010	JA - OMA (1800 g/mm)	H_β

6 DATA ANALYSIS AND RESULTS

6.1 Wavelength Calibration and Sensitivity Correction

The relative spectral sensitivity – or the response of the detector over the spectral range of interest – of the data acquisition system is obtained by using a tungsten-strip lamp. By comparing the recorded tungsten emission to its actual profile, as provided by the lamp manufacturer, we are able to determine the sensitivity of the system for a given experimental configuration (i.e., optics, filters, windows, gratings and detectors). The data files are sensitivity-corrected by dividing the experimental spectrum by the relative spectral sensitivity.

The response of the linear diode array is specified by the manufacturer to be linear within one percent. To confirm such accurate response, precise measurements are required using calibrated neutral density filters and a constant radiation source. In the process of sensitivity calibration the linear response specification was checked for similar OMA acquisition parameters as used in the measurements for the hydrogen Balmer spectra. The linearity of the photomultiplier has been verified in experiments accomplished outside this thesis.

Wavelength calibration is accomplished by a cubic polynomial fit to atomic lines from calibration lamps intended for this purpose. Detector dark-noise, due to the internal electronics of the detector controller, and any background light that may accumulate during data acquisition was subtracted from the data at the time they were acquired.

6.2 Electron Temperature

6.2.1 Boltzmann Plot Analysis

We use low resolution data for the Boltzmann plot estimation of electron temperature. As can be seen in Fig. 7, the Balmer lines are so wide at early times that individual lines of the series are not isolated from one another. The wings of one line superimpose the profiles of the other lines. As the plasma decays, and the electron density decreases, the lines become narrower and individual lines begin to emerge from the continuum – first the H_α, then the H_β, then the H_γ and so on. As each line becomes independent from adjacent lines, that is, when the wings of adjacent lines do not contribute significantly to the intensity of the line of interest, that line is included in the Boltzmann plot. Obviously, then, Boltzmann plots cannot be used at very early times since only the H_α line is discernable. The first Boltzmann plots contain only two lines – H_α and H_β – and provide, at best, only an estimate of the temperature. As time passes more lines can be included in the Boltzmann plot yielding a more accurate temperature. Typical Boltzmann plots are shown in Fig. 8.

The Boltzmann plot data were taken using the J-A spectrometer with the 150 g/mm grating and a cell pressure of 810 torr and 1010 torr. The data were wavelength and sensitivity corrected as described above. The intensities of the Balmer lines as well as which lines to include in the Boltzmann plot were determined by inspection (i.e., by plotting the data). The Boltzmann plots are accomplished through a least squares linear regression routine, and the uncertainty in the temperature is inferred

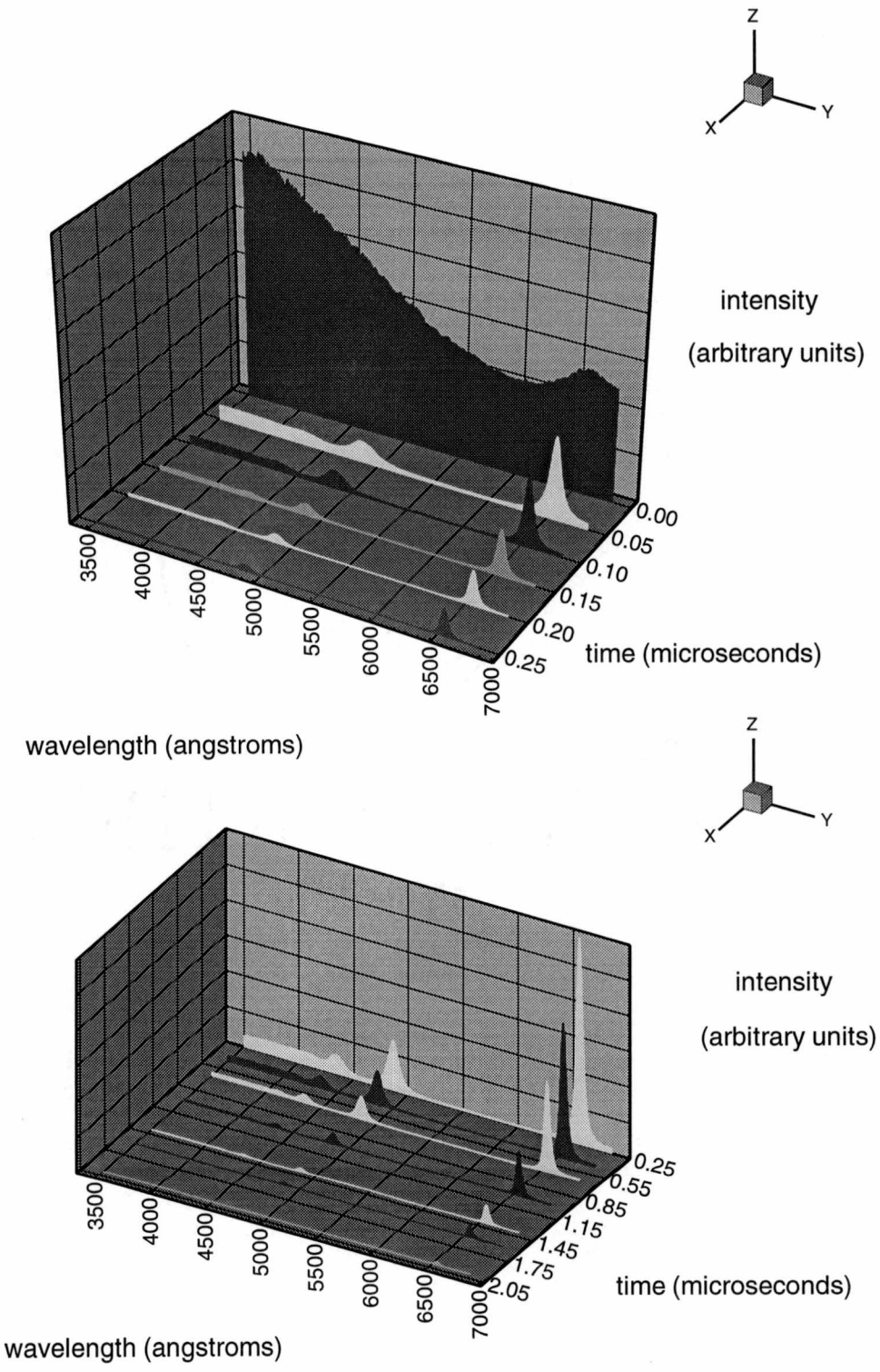

Figure 7: Time evolution of the hydrogen Balmer series, 0 to 2 μs

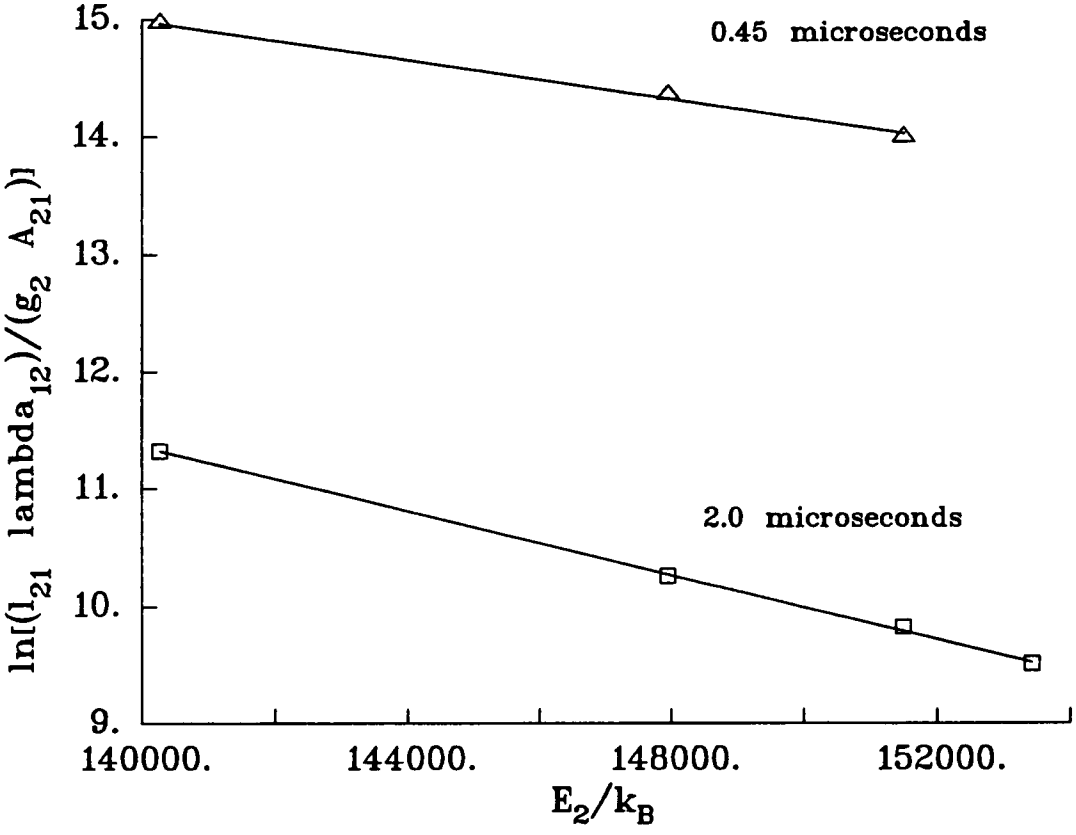

Figure 8: Boltzmann plots for time delays of 0.45 and 2.0 μs

from the standard deviation in the slope of the resulting straight line fit using

$$\Delta T = \frac{\Delta slope}{(slope)^2} = T^2 \sigma_{slope}, \tag{7}$$

where $\Delta slope = \sigma_{slope}$ = standard deviation.

6.2.2 Boltzmann Plot Results

The results of the Boltzmann plots are summarized in Tables 3 and 4. The electron temperatures are plotted versus time in Figs. 9 and 10. These figure show the electron temperature decay for the two cell pressures. At early times, t $<$ 250 ns, the results suggest that the electron temperature is higher for the higher pressure case. However, for subsequent times the two temporal profiles are essentially the same up to delays of 1.6 μs. There are two interesting features of these results that should be noted: the temperature minimum that occurs at 300 ns and the differences in the results for t $\geq$ 2μs. It is believed that the source of these two anomalies lies in spatial inhomogeneities of the plasma.

No attempt has been made in the previous data acquisition or analysis to resolve spatially the plasma emission. We optimized the optical arrangement for maximum throughput of the signal to the detector without consideration of where in the laser spark we were looking. Our objective was to obtain a spatial average of the desired parameters.

It is recognized, however, that spatial inhomogeneities exist in the plasma formation and subsequent decay. Some, if not all, of the irregularities that we see in the

Table 3: Boltzmann plot temperatures for 810 torr cell pressure

Time (μs)	Temperature (K)	uncertainty	lines include
0.05	13,118	–	H_α, H_β
0.10	13,031	–	H_α, H_β
0.15	13,221	1044	H_α, H_β, H_γ
0.20	12,226	200	H_α, H_β, H_γ
0.25	11,759	111	H_α, H_β, H_γ
0.30	11,677	368	H_α, H_β, H_γ
0.35	11,722	509	H_α, H_β, H_γ
0.40	11,621	550	H_α, H_β, H_γ
0.45	11,626	701	H_α, H_β, H_γ
0.50	11,498	761	H_α, H_β, H_γ
0.55	11,532	736	H_α, H_β, H_γ
0.60	11,278	819	H_α, H_β, H_γ
0.65	11,394	813	H_α, H_β, H_γ
0.70	10,320	477	H_α, H_β, H_γ
0.75	10,975	736	H_α, H_β, H_γ
0.80	10,907	719	H_α, H_β, H_γ
1.0	10,645	873	H_α, H_β, H_γ
1.2	10,341	700	H_α, H_β, H_γ
1.4	10,088	436	H_α, H_β, H_γ
1.6	9766	242	H_α, H_β, H_γ
2.0	7348	161	H_α, H_β, H_γ
2.5	6028	513	H_α, H_β, H_γ
3.0	6010	104	H_α, H_β, H_γ

Table 4: Boltzmann plot temperatures for 1010 torr cell pressure

Time (μs)	Temperature (K)	uncertainty	lines include
0.10	13,678	–	H_α, H_β
0.15	13,193	–	H_α, H_β
0.20	13,099	–	H_α, H_β
0.25	11,858	101	H_α, H_β, H_γ
0.30	11,534	258	H_α, H_β, H_γ
0.35	11,542	410	H_α, H_β, H_γ
0.40	11,601	542	H_α, H_β, H_γ
0.45	11,644	624	H_α, H_β, H_γ
0.50	11,506	673	H_α, H_β, H_γ
0.55	11,318	811	H_α, H_β, H_γ
0.60	11,311	809	H_α, H_β, H_γ
0.65	11,145	843	H_α, H_β, H_γ
0.70	11,120	888	H_α, H_β, H_γ
0.75	10,918	850	H_α, H_β, H_γ
0.80	10,912	906	H_α, H_β, H_γ
1.0	10,540	878	H_α, H_β, H_γ
1.2	10,296	829	H_α, H_β, H_γ
1.4	9931	661	H_α, H_β, H_γ
1.6	9506	414	H_α, H_β, H_γ, H_δ
2.0	8961	296	H_α, H_β, H_γ, H_δ
2.5	9009	217	H_α, H_β, H_γ, H_δ
3.0	8772	228	H_α, H_β, H_γ

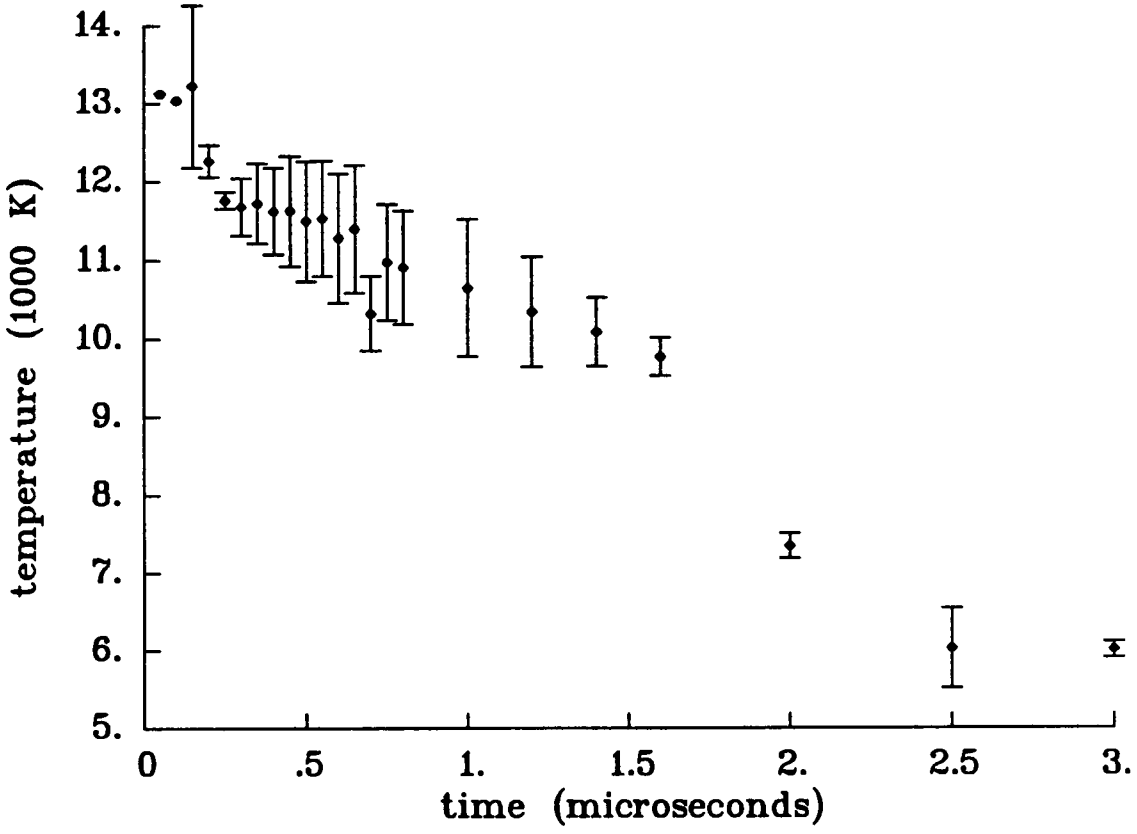

Figure 9: Electron temperatures for a cell pressure of 810 torr

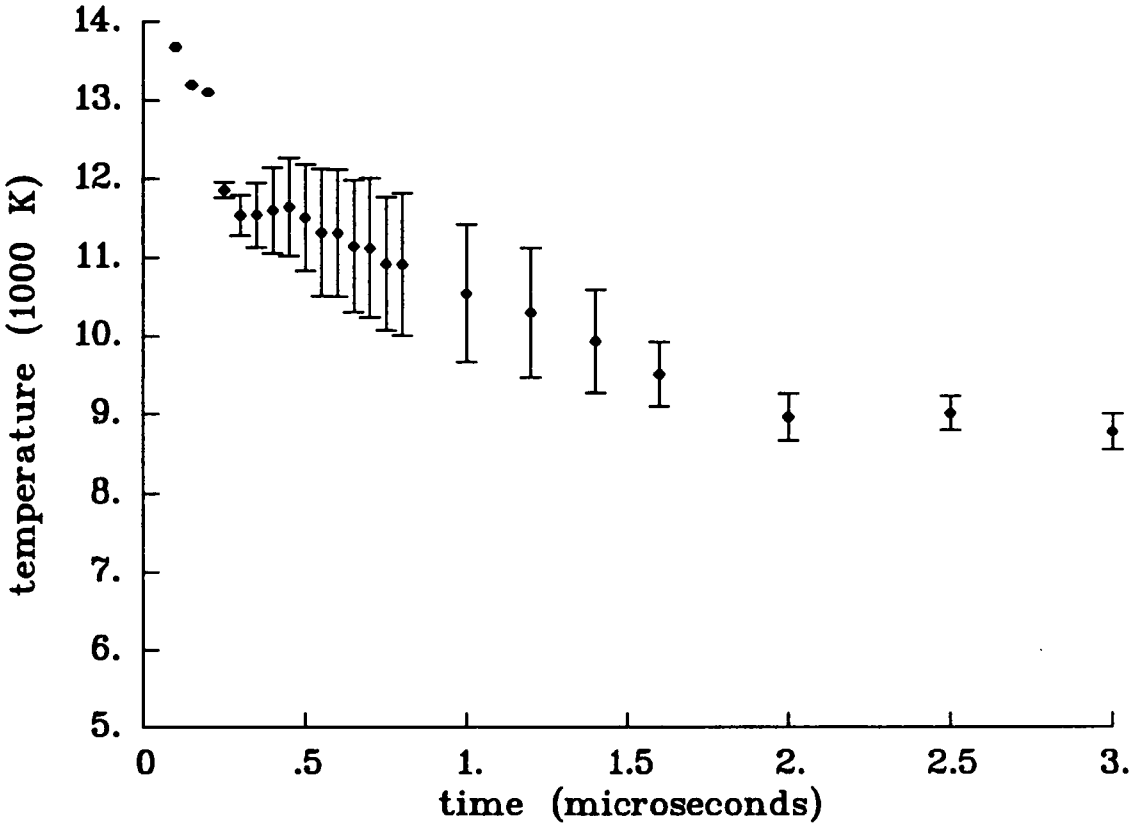

Figure 10: Electron temperatures for a cell pressure of 1010 torr

Boltzmann plot results are certainly attributable to these inhomogeneities. Further discussion on plasma inhomogeneities is contained in Chapter 7.

6.3 Electron Density

The data analysis for electron density is accomplished by two methods. One involves the measured full width at half maximum width parameter of the spectral line, and the other utilizes the full experimental spectral profile. Typical experimental H_α and H_β profiles at various time delays are shown in Figs. 3 and 4 on pages 14 and 15. Note the extreme width of both lines at early time delays.

6.3.1 Electron Number Density from Line Widths

The first method measures the FWHM of the emission line and uses this measured value to infer electron number density. In the cases where the profiles are noisy the peaks are smoothed to assist in determination of the peak intensity. The experimental profiles are then normalized. The FWHM is determined by interpolating a three term polynomial fit through the five points nearest the half height on the blue and red sides of the hydrogen line. For high electron number densities the H_β line has an intensity asymmetry between its two peaks. In such cases, the peak used for determining the FWHM is taken as the average intensity of the two peaks. The contribution of the spectrometer entrance slit to the FWHM of the hydrogen lines is corrected for as described in Appendix B. The electron density is then determined from the FWHM by essentially using Eq. (3). However, instead of using this equation directly we use

tabulated theoretical results.

Griem's Table AIIIa [11] gives a compilation of FWHM as a function of temperature and electron density. The electron density for a given line width can be determined from this table by interpolating between the given elements. The variation of FWHM with temperature at a given electron density is very small. Therefore a linear interpolation is sufficient for temperature. The FWHM varies as $N_e^{2/3}$ and is interpolated accordingly. Figures 11 and 12 show the temperature and density variation of the H_α FWHM. Figures 13 and 14 show the temperature and density variation of the H_β FWHM. Also shown in Figs. 11 and 13 are the $N_e^{2/3}$ interpolation results.

In the case of the H_α line we apply ion-dynamical corrections [12] to Griem's theoretical FWHM's. In Griem's calculations, the ion perturbers are assumed to behave quasi-statically. The broadening calculations are performed by averaging over the static electric micro-field produced by the ions. This approximation gives good results for higher electron number densities. For electron number densities less than $\sim 10^{17}$ cm^{-3}, the ion dynamic contribution to the collisional broadening of the H_α line cannot be ignored. For a given line width this correction results in a lower inferred electron number density. As can be seen from Fig. 15, the ion-dynamical corrections are only important for electron densities less than 10^{17} cm^{-3}.

The line width method is used for the analysis of all J-A data since the slit function contribution to the recorded profile is significant in the electron density

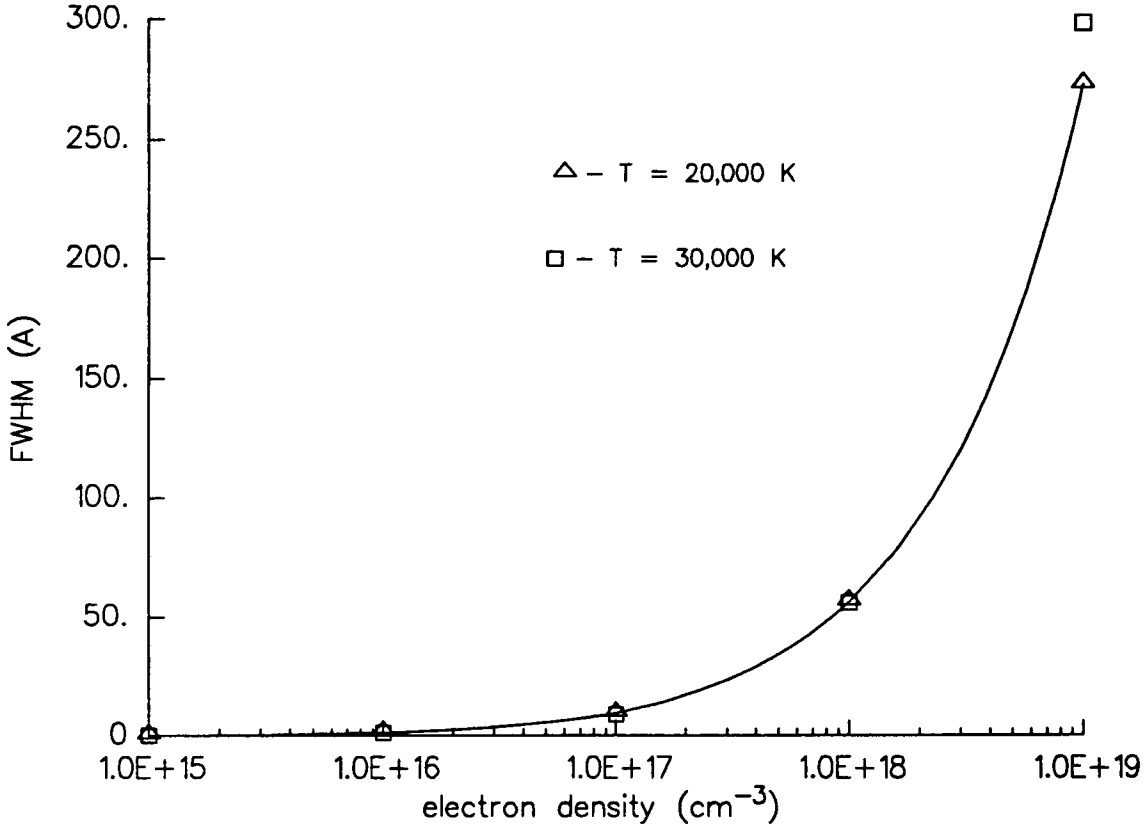

Figure 11: H_α line widths for temperatures of 20,000 K and 30,000 K and a $N_e^{2/3}$ interpolation result

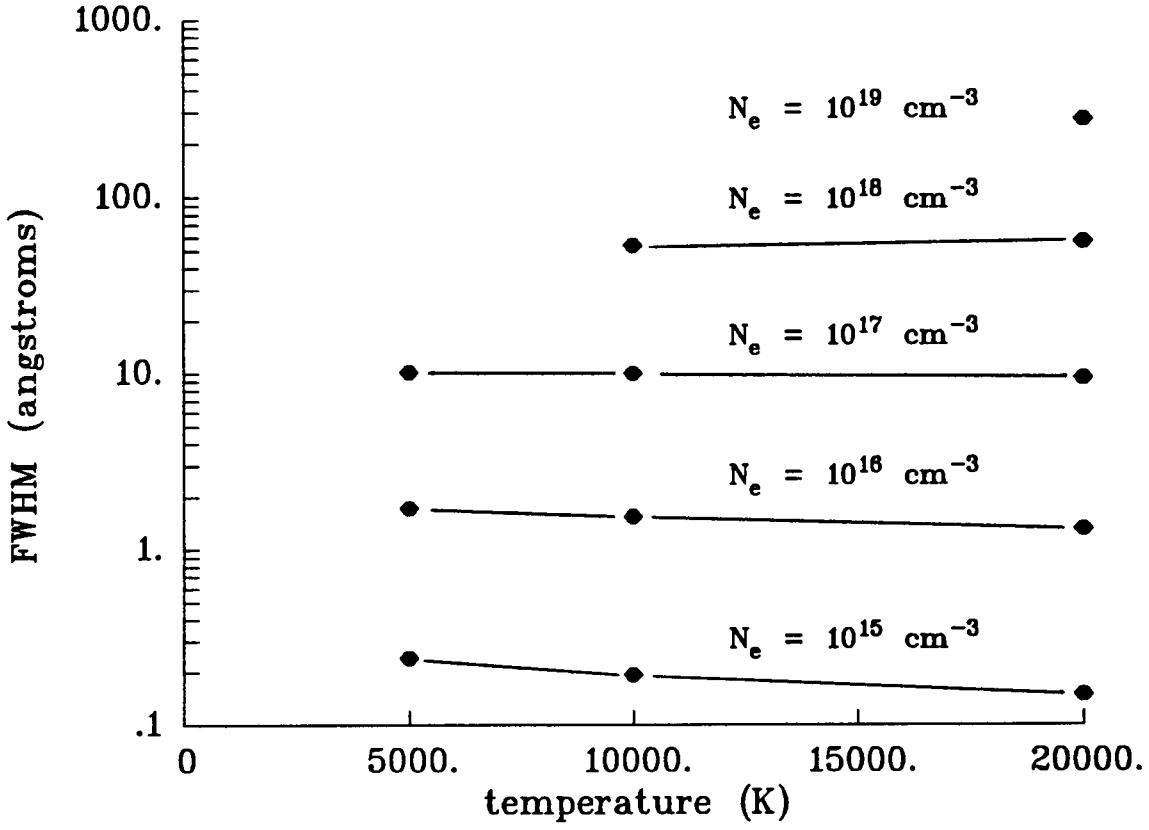

Figure 12: Tabulated H_α FWHM's for temperatures of 5,000, 10,000 and 20,000 K

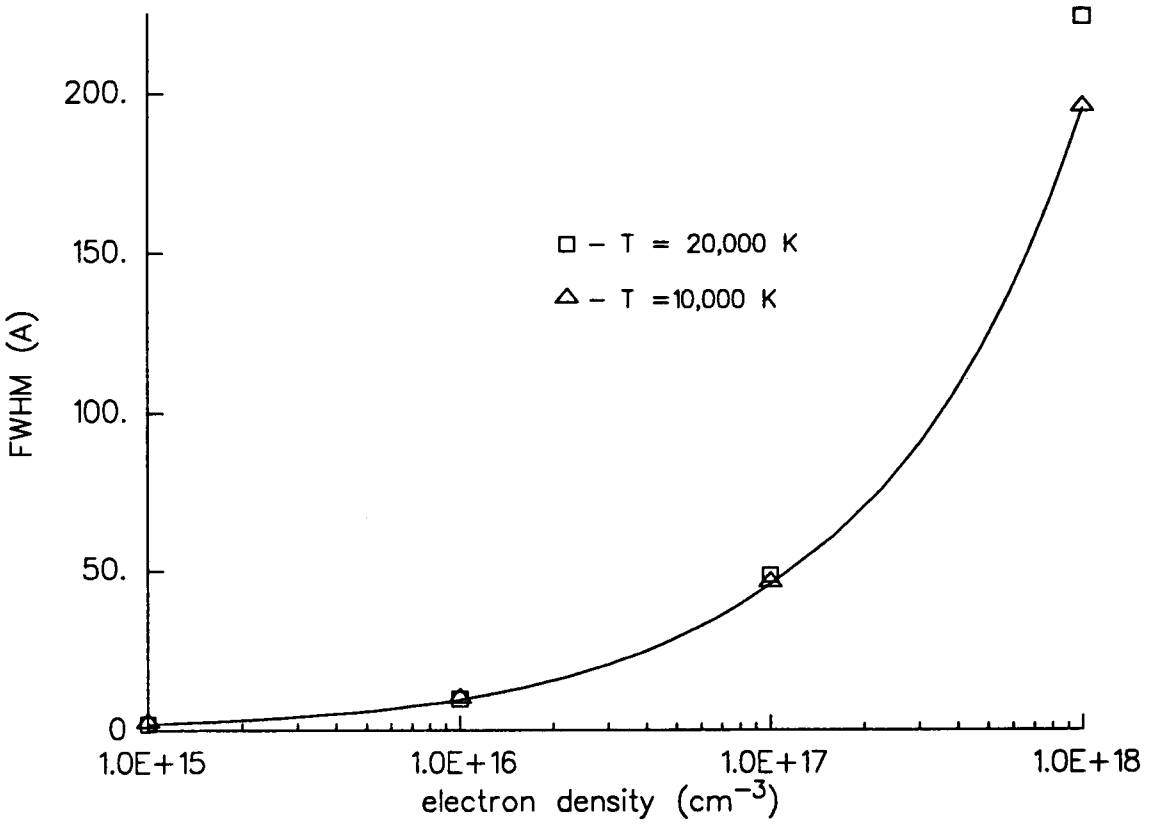

Figure 13: H_β line widths for temperatures of 10,000 K and 20,000 K and a $N_e^{2/3}$ interpolation result

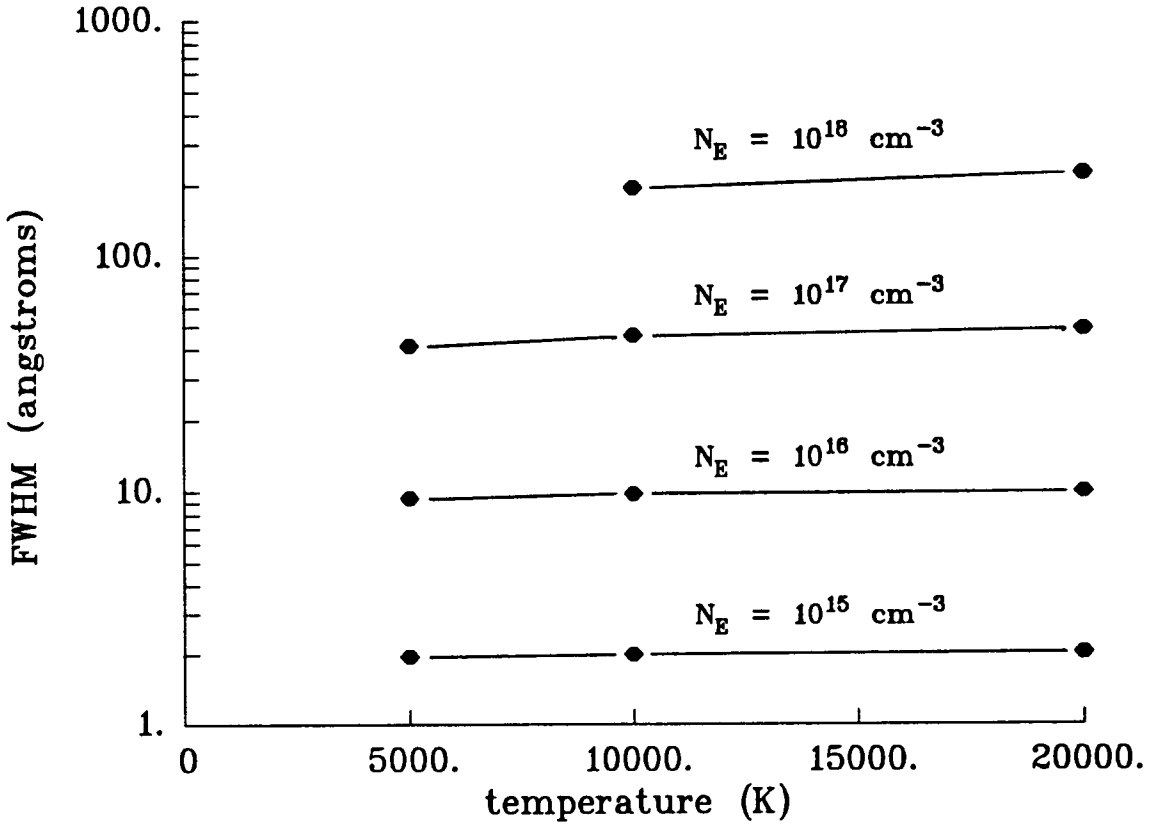

Figure 14: Tabulated H_β FWHM's for temperatures of 5,000, 10,000 and 20,000 K

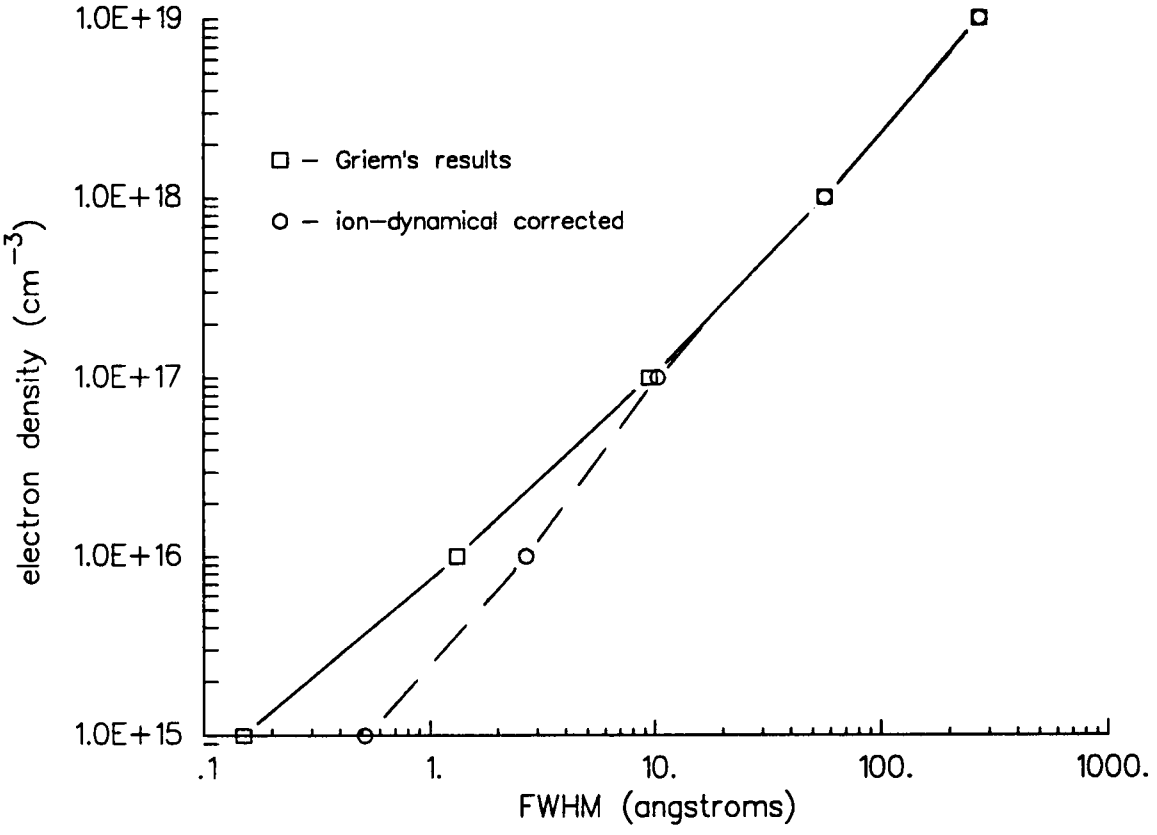

Figure 15: Uncorrected and ion-dynamical corrected FWHM's

range covered by these data sets. These data sets include both H_α and H_β profiles. This technique allows for small corrections that can be obtained from the knowledge of electron temperatures that we obtain from the Boltzmann plot results as well as the ion-dynamical corrections that become more significant at lower electron densities.

6.3.2 Electron Number Density from Full Profile Fit

The second method uses Griem's tabulated theoretical line profiles to fit experimental H_α profiles. Since the profile of a given H_α line is a weak function of temperature, we assume a temperature to fit the data, where the Boltzmann plot results are again used as a guide to the selection of which temperature to use in this analysis scheme.

Since the tabulated profiles are only given for densities of $10^{15}, 10^{16}, 10^{17}$, 10^{18} and 10^{19} cm^{-3}, we use an interpolation scheme, based on the $N_e^{2/3}$ dependence of the FWHM, to fit profiles that are within one order of magnitude. The experimental profiles are fit using four fitting parameters. The profiles are compared to a combination of the theoretical profile at a given electron density plus a wavelength shift superimposed on a straight line of variable slope and variable intensity offset. While the electron density and the shift are varied, the straight line slope and intensity offset are optimized through a least-squares regression. The density and shift are passed through a grid of evenly spaced points. The results are tabulated, and the criterion for the best fit is the minimum sum of square errors (SSE). Figure 16 is a plot of the SSE over a typical grid of line shifts and electron densities and shows that there is a unique minimum.

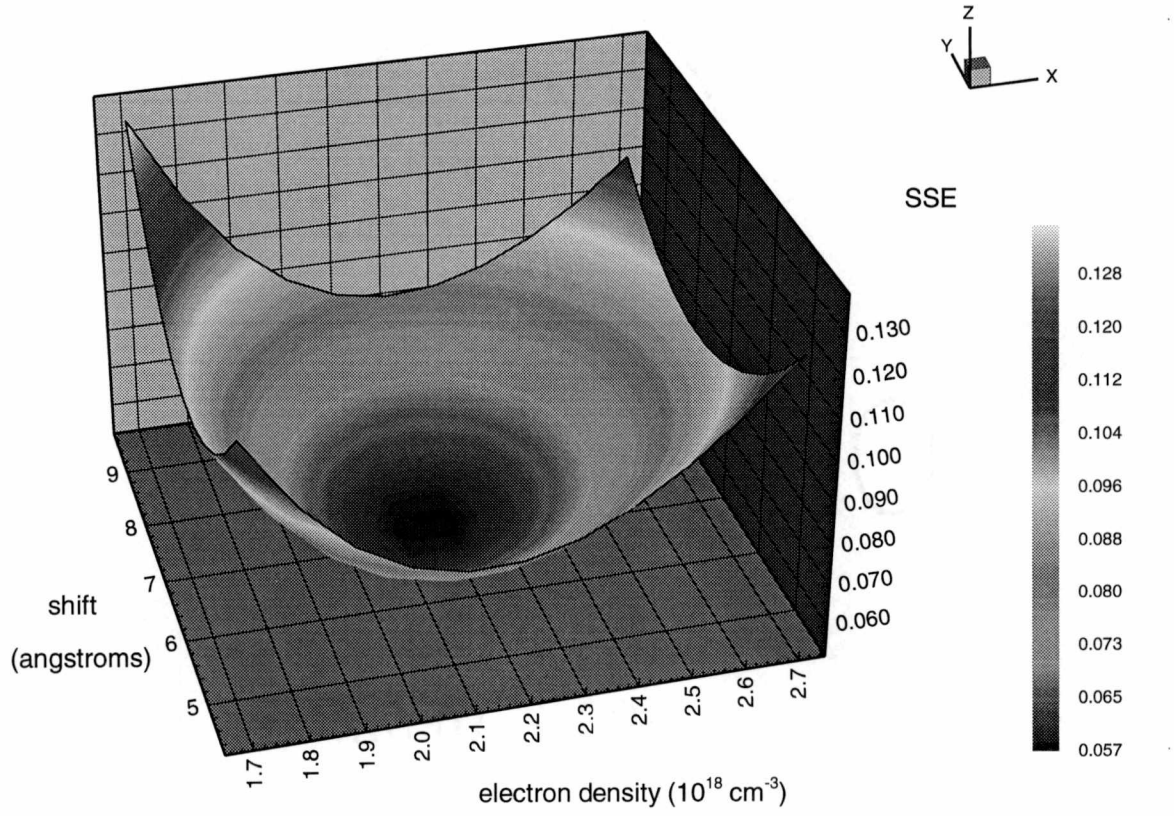

Figure 16: Plot of the SSE's over a typical electron density and wavelength shift grid

In the fitting procedure the offset is used to correct for an overall background contribution while the slope is used to account for a linear wavelength dependence of the background. Both offset and slope can be a measure for electron density and temperature provided that complete profiles are recorded without contributions from other lines, for example, from the H_β wing. It was found that the offset and slope are very susceptible to the sensitivity correction that was applied to the experimental spectra. Therefore, the fitted offset and slope are not a good measure for electron density and temperature in the experimental data sets. Including these two parameters, however, generally improves the fit in terms of the SSE. Experimental profiles, fitted profiles and residuals are shown in Figs. 17 – 19. As can be seen from the figures, the agreement is quite good. The overall profile matches very well with the major discrepancies being at the peak and in the wings.

6.3.3 Results

The electron density results of both methods for H_α at 810 torr are listed in Table 5 and plotted in Figs. 20 and 21. The first figure shows the two stages of electron density decay before and after 100 ns. The second figure uses a logarithmic y-axis to enhance detail. In the region of overlap there is good agreement between the two methods except for the factor of 2 difference at 2 μs delay. In this figure the BOXCAR data files are analyzed using full profile fits and the OMA results come from FWHM inference.

Figure 22 and Table 6 and show a comparison between the two methods for

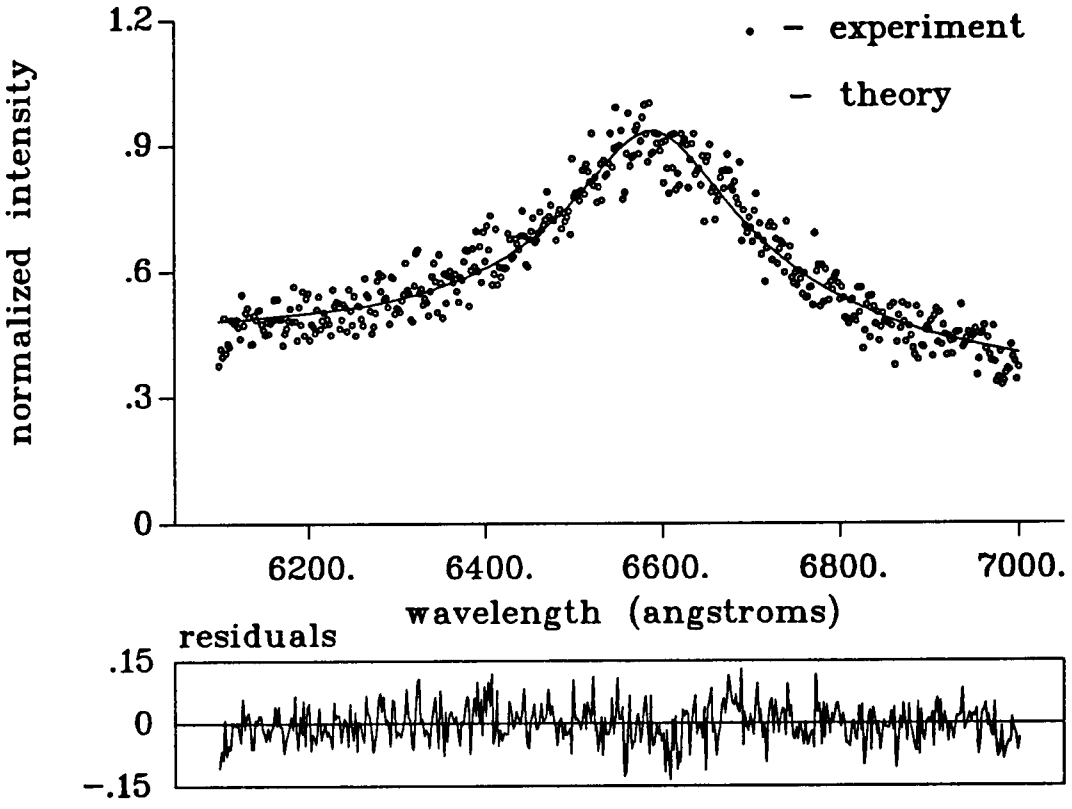

Figure 17: H_α experimental profile, fitted profile and residuals at a delay of 5 ns and a cell pressure of 810 torr

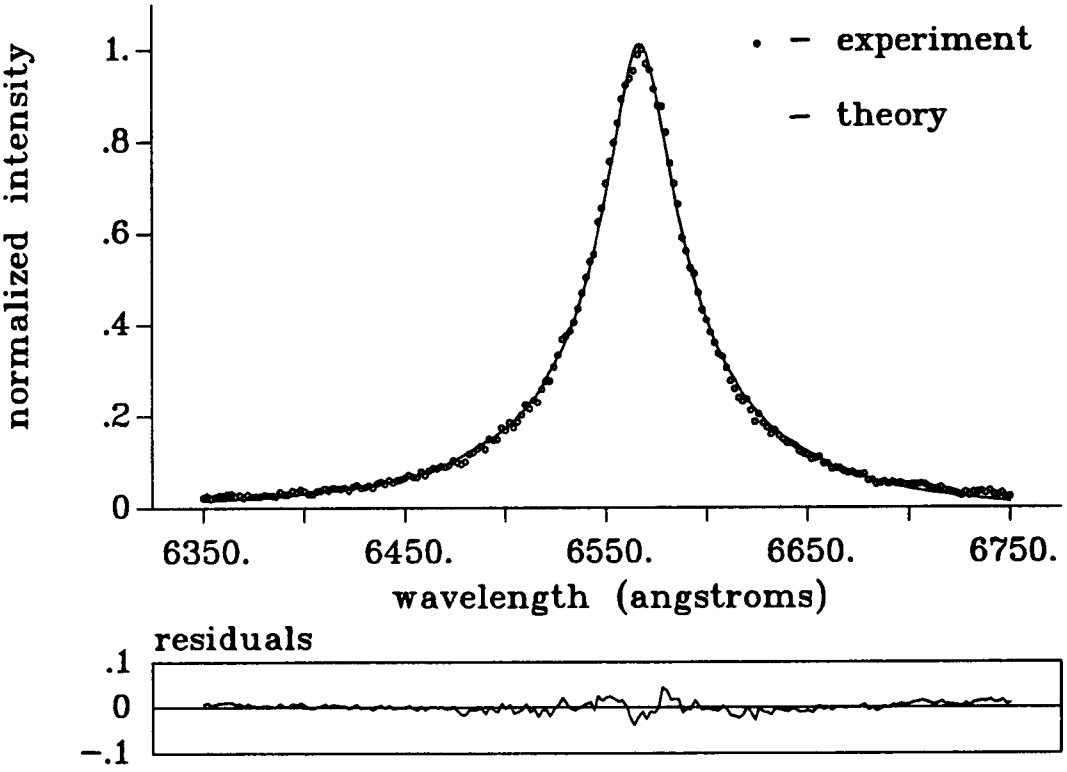

Figure 18: H_α experimental profile, fitted profile and residuals at a delay of 100 ns and a cell pressure of 810 torr

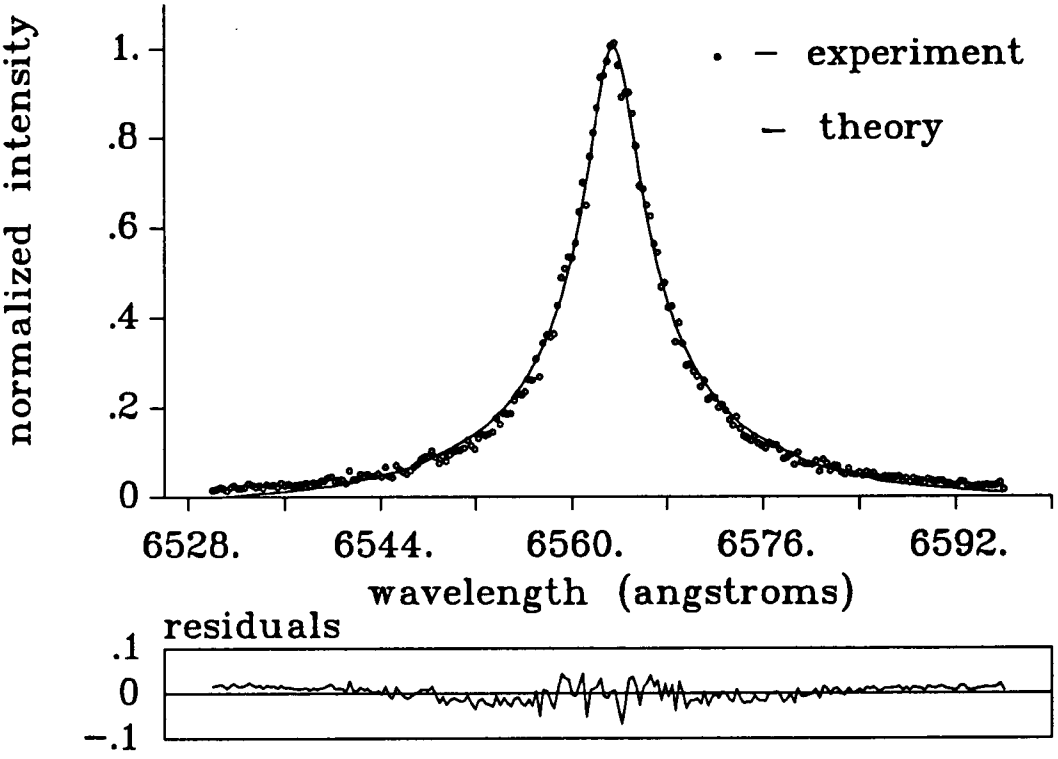

Figure 19: H_α experimental profile, fitted profile and residuals at a delay of 1 μs and a cell pressure of 810 torr

Table 5: Electron densities from full profile fit (BOXCAR) and FWHM (OMA) of the H_α line at a cell pressure of 810 torr

time delay (μs)	N_e (full profile)	N_e (FWHM)
0.005	1.1×10^{19}	
0.02	5.4×10^{18}	
0.04	2.7×10^{18}	
0.06	2.1×10^{18}	
0.08	1.3×10^{18}	1.18×10^{18}
0.10	1.0×10^{18}	9.35×10^{17}
0.15		5.81×10^{17}
0.25		3.25×10^{17}
0.35		2.30×10^{17}
0.45	2.0×10^{17}	1.83×10^{17}
0.55		1.63×10^{17}
0.65		1.26×10^{17}
0.75		1.00×10^{17}
0.85		1.00×10^{17}
0.95		8.79×10^{16}
1.00	7.1×10^{16}	
1.05		7.90×10^{16}
1.25		6.57×10^{16}
1.45		5.28×10^{16}
1.65		4.20×10^{16}
1.95		3.07×10^{16}
2.00	1.4×10^{16}	
3.05		4.43×10^{15}

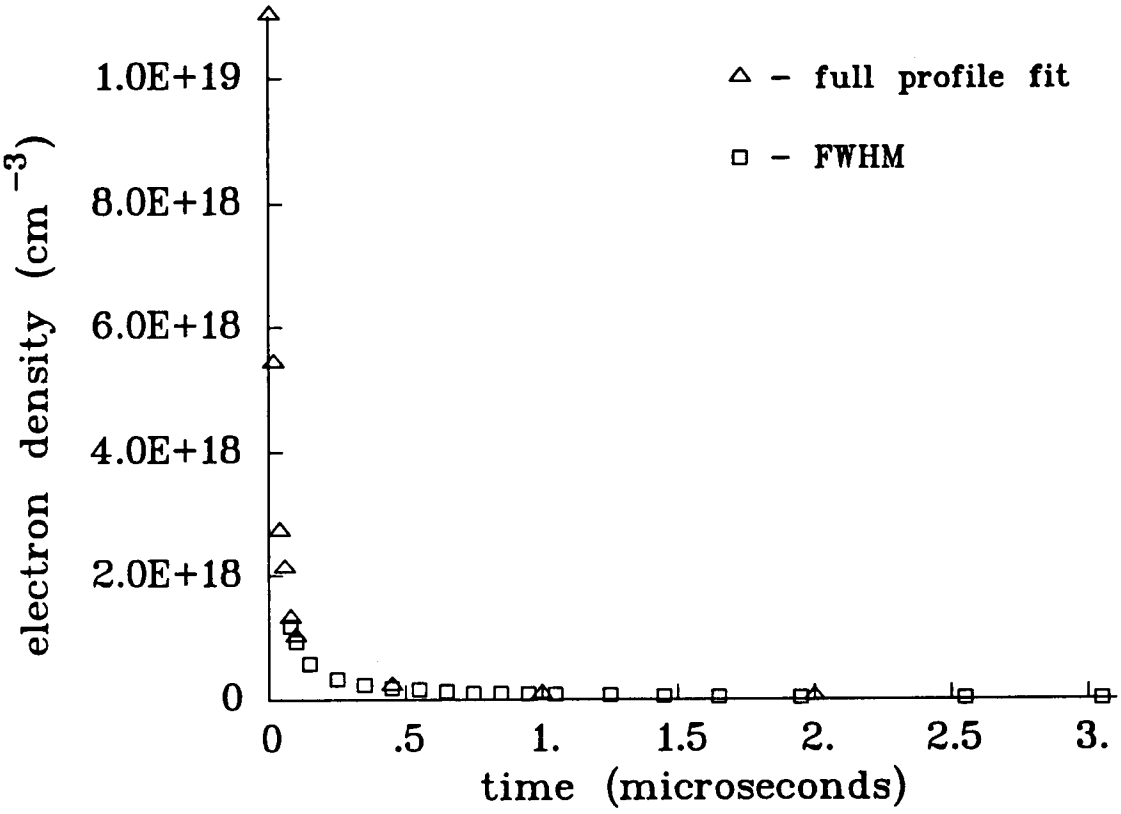

Figure 20: Electron densities from H_α lines for a cell pressure of 810 torr

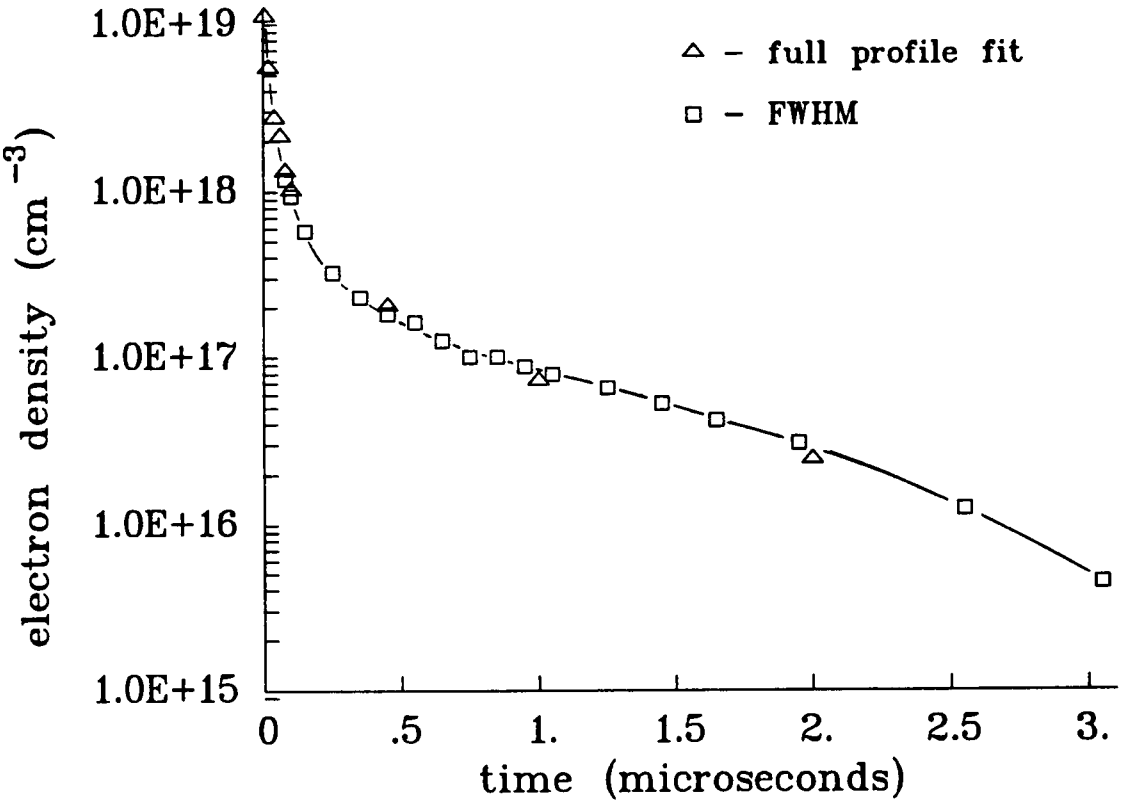

Figure 21: Electron densities from H_α lines for a cell pressure of 810 torr

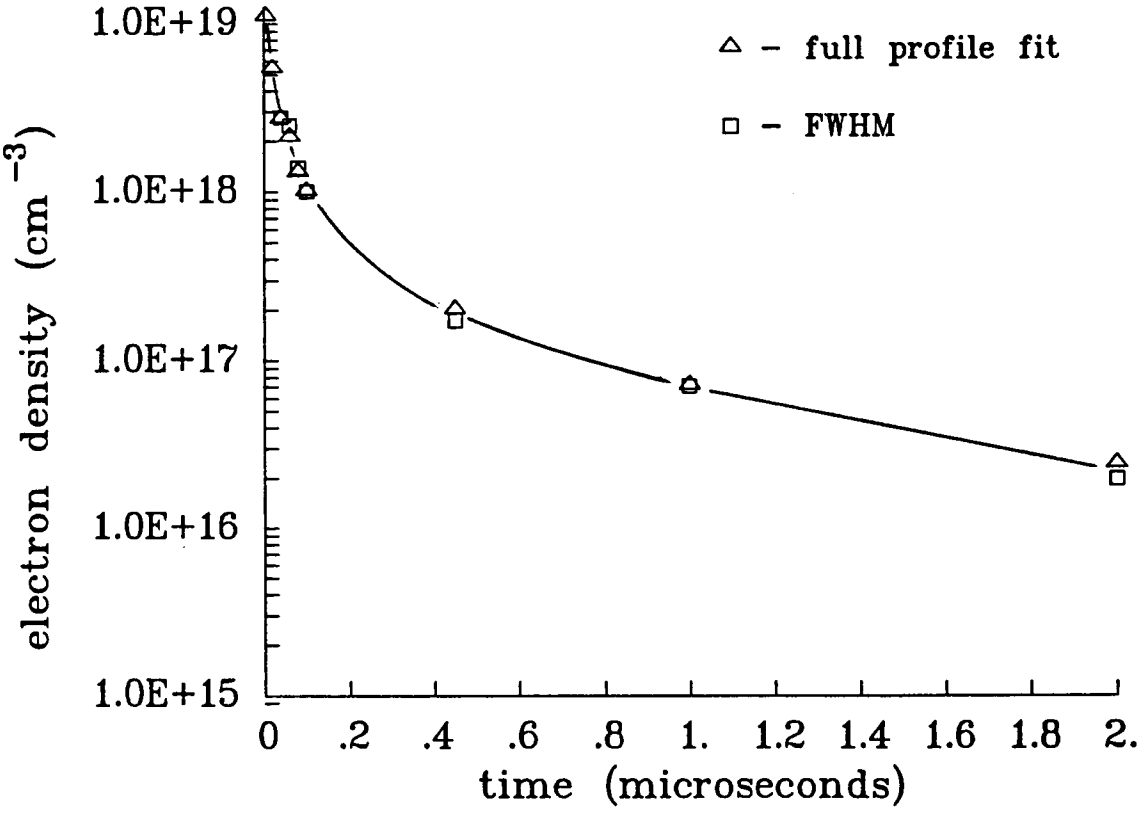

Figure 22: Comparison of the full profile fitting method and the FWHM method with the H_α line at 810 torr

Table 6: Electron densities from the full profile fit and FWHM of the H_α line at a cell pressure of 810 torr applied to the BOXCAR data

time delay (μs)	N_e (full profile)	N_e (FWHM)	ratio
0.04	2.8×10^{18}	2.7×10^{18}	1.04
0.06	2.5×10^{18}	2.1×10^{18}	1.19
0.08	1.4×10^{18}	1.3×10^{18}	1.08
0.10	1.0×10^{18}	1.0×10^{18}	1.0
0.45	1.7×10^{17}	2.0×10^{17}	0.85
1.00	7.1×10^{16}	7.1×10^{16}	1.0
2.00	2.0×10^{16}	2.4×10^{16}	0.83

BOXCAR data in the first 2 μs of the plasma decay. Again, the agreement between the two methods is good, as it should be since the two methods should yield similar results for the same data set. For plasma decay times less than 100 ns the full profile fit is likely to yield the better result due to the following reasons: (1) The H_α line is so wide that the entire profile is difficult to record, thus the profiles are incomplete. (2) The H_α profile is distorted due to contributions from the H_β wing and the underlying continuum. Full profile fitting yields better results in this case since the fitting procedure does not assume a complete profile nor does it assume a flat background.

Figure 23 shows the electron density results from H_α and H_β for a cell pressure of 810 torr where we have used the line widths to infer electron densities. The agreement between the two lines is good out to 0.5 microseconds at which point they start to diverge. At 0.75 μs the ratio of the two electron densities, $(N_e)_{H_\alpha}/(N_e)_{H_\beta}$, is 1.2. At 1.5 μs the ratio is 2.0, and at 2.5 μs it is 5.4. Theoretical results [11] tell us that we

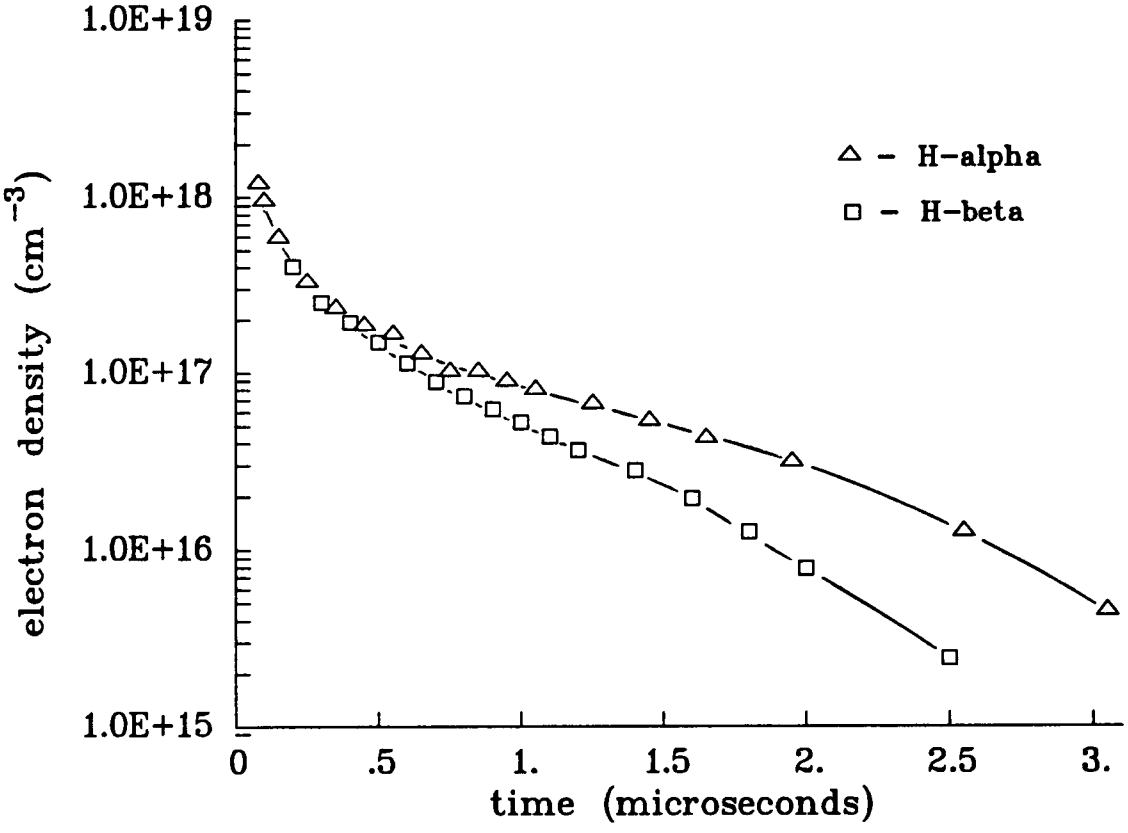

Figure 23: Comparison of H_α results with H_β results at 810 torr

can expect electron density accuracies of at best 5 % for H_β and 20 % for H_α.

The comparison above shows that our results fall well out of this range and suggest a systematic, or experimental, error. The magnitude of the disparity at later times, and the increase with time, suggest that once again we are seeing spatial inhomogeneities in the plasma. The data represent the results of two separate experimental arrangements where different optical arrangements were used to image the plasma onto the spectrometer slit. The H_α profiles were obtained using two 10 cm focal length lenses: one to collimate the signal and one to focus it onto the spectrometer slit. The H_β profiles were obtained by positioning the gas cell closer to the spectrometer and using a single lens to image the breakdown onto the entrance slit. Schematic drawings of the two optical arrangements, which show a projection of the spectrometer slit onto the plasma, are shown in Fig. 6.

Electron densities for cell pressures of 810 torr and 1010 torr are shown in Fig. 24. These results are from H_β line widths. If we divide the electron densities at 1010 torr by those at 810 torr we see that the result is not a straight line. This result is shown in Fig. 25 and Table 7. We can see from Fig. 24 that there is a definite increase in electron number density with an increase in pressure, as expected.

The anticipated increase in electron number density can be estimated using the ideal gas law. Approximating H_2 gas as an ideal gas we get

$$n_2 = n_1 \cdot P_2/P_1 \tag{8}$$

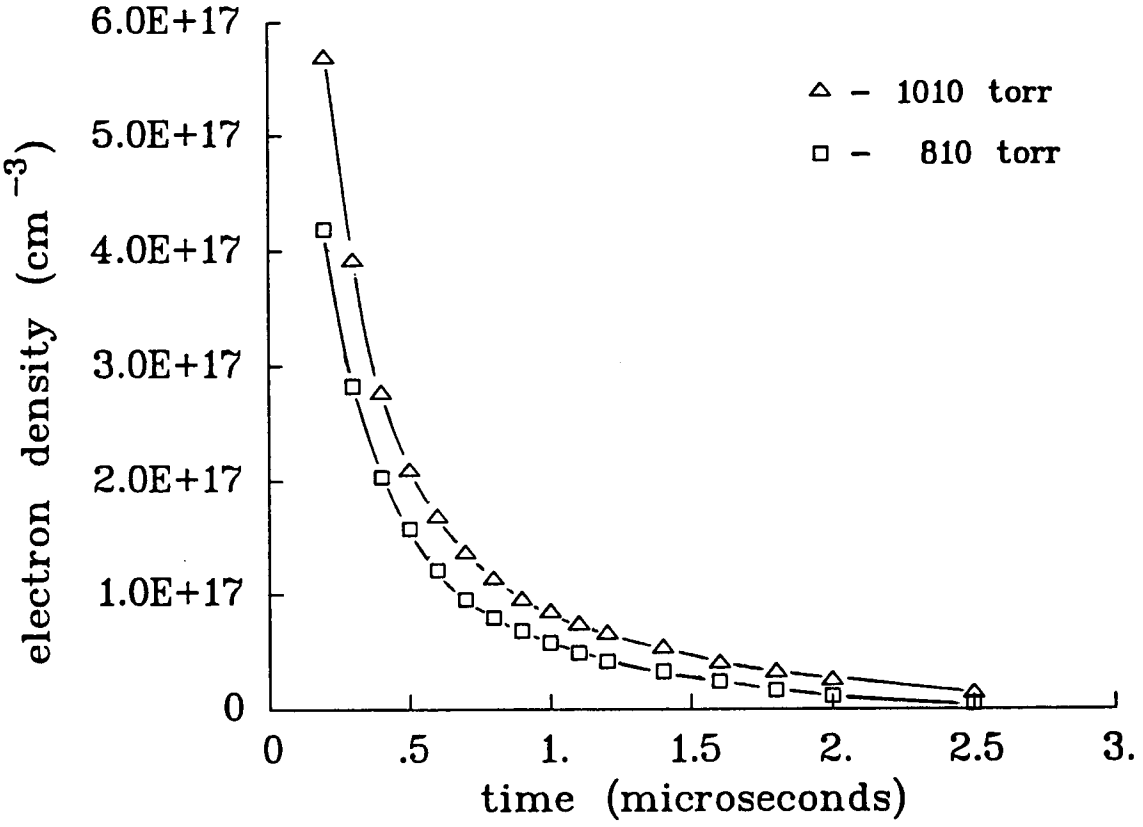

Figure 24: H_β electron densities at 810 and 1010 torr

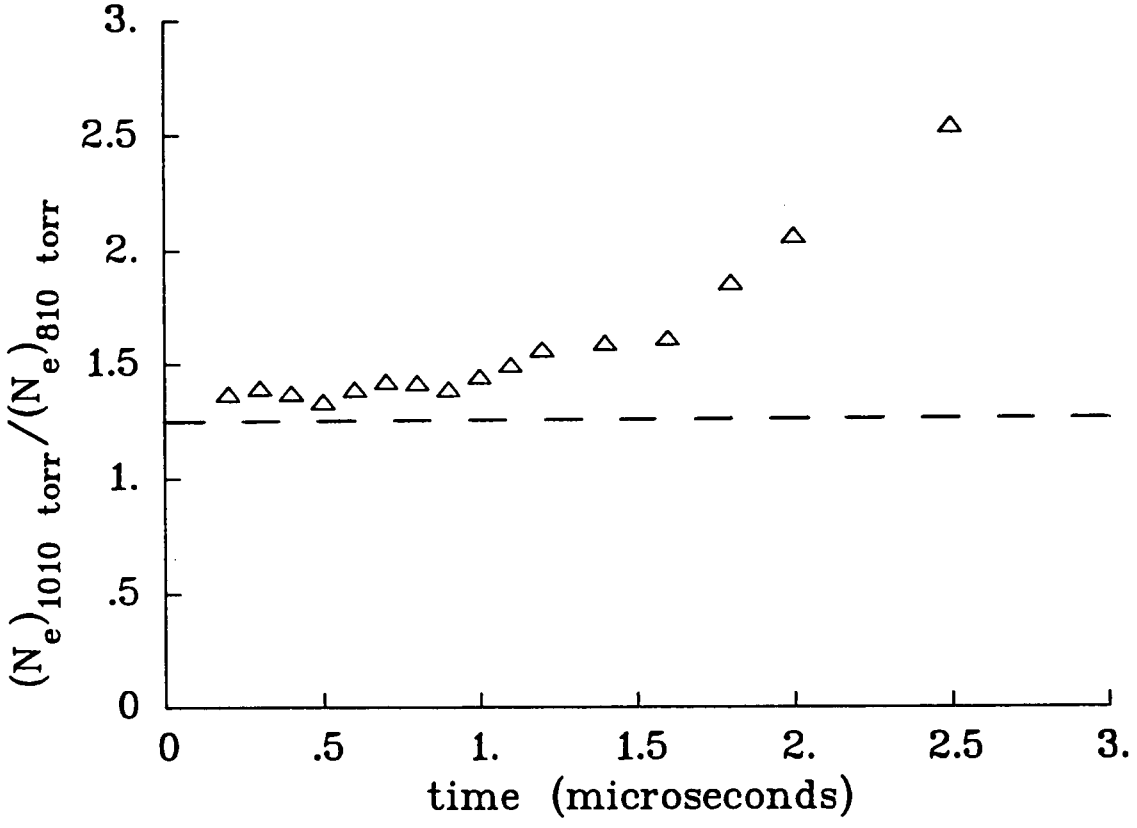

Figure 25: Electron density at 1010 torr divided by electron density at 810 torr

Table 7: Electron densities from H_β FWHM's at cell pressures of 810 and 1010 torr

time delay (μs)	N_e (1010 torr)	N_e (810 torr)	ratio
0.2	5.55×10^{17}	4.07×10^{17}	1.36
0.3	3.79×10^{17}	2.53×10^{17}	1.50
0.4	2.66×10^{17}	1.94×10^{17}	1.37
0.5	1.98×10^{17}	1.49×10^{17}	1.33
0.6	1.58×10^{17}	1.14×10^{17}	1.39
0.7	1.26×10^{17}	8.90×10^{16}	1.42
0.8	1.03×10^{17}	7.37×10^{16}	1.40
0.9	8.68×10^{16}	6.25×10^{16}	1.42
1.0	7.64×10^{16}	5.26×10^{16}	1.45
1.1	6.62×10^{16}	4.37×10^{16}	1.51
1.2	5.83×10^{16}	3.65×10^{16}	1.60
1.4	4.38×10^{16}	2.82×10^{16}	1.55
1.6	3.31×10^{16}	1.96×10^{16}	1.69
1.8	2.59×10^{16}	1.27×10^{16}	2.04
2.0	1.90×10^{16}	7.90×10^{15}	2.41
2.5	8.10×10^{15}	2.45×10^{15}	3.31
2.5	8.45×10^{15}	–	–

For $P_1 = (810 \pm 25)$ torr and $P_2 = (1010 \pm 25)$ torr we find

$$n_2 = n_1 \cdot (1.25 \pm 0.07) \tag{9}$$

The electron density ratios are slightly larger than the upper limit of this range at early times, out to about one microsecond. For later times, the ratios differ significantly from the expected values. We would expect to see a decrease in the recombination rate and a slower relaxation of the electron density at higher pressure if the electron temperatures were higher. The Boltzmann plots show that the electron temperatures at the two pressures are approximately the same. This result suggest that: (1) the simple increase in pressure argument is inadequate, (2) we are observing different regions of the plasma as it decays, (3) we see the combined effects of these two

possibilities.

As mentioned earlier, the wavelength separation between the red and blue peak of the H_β line is a function of the electron density. Theoretical considerations suggest that the correlation is

$$\lambda_R - \lambda_B = a \cdot \Delta\lambda_{1/2} \tag{10}$$

The theoretical results of Seidel [22] suggest that $a = 0.35$ and those of Kudrin and Sholin [23] give $a = 0.18$. The experimental results of Helbig and Nick [9] and those of Uhlenbusch and Viöl [16] agree more closely to Seidel's result.

Using Eq. (10) we determine the value of a for our experimental data. The results are summarized in Table 8 and plotted in Fig. 26. The resulting average value, a = 0.26, falls almost exactly in the middle of Seidel's result and Kudrin and Sholin's result.

One might explain this discrepancy in the parameter a in terms of a spatial average of the plasma emission. We know that spatial inhomogeneities exist in the laser-induced plasma. Therefore, we expect the detector to see regions of various electron

Table 8: H_β peak separation correlation to FWHM - 810 torr

time delay (μs)	FWHM (Å)	$\lambda_R - \lambda_B$	a	e^- density (cm^{-3})
0.1	207.1	50.0	0.241	1.05×10^{18}
0.2	114.1	29.0	0.254	4.19×10^{17}
0.3	88.44	23.1	0.261	2.83×10^{17}
0.4	71.80	19.3	0.269	2.03×10^{17}
0.5	61.09	16.2	0.265	1.57×10^{17}
0.6	51.98	15.1	0.291	1.21×10^{17}

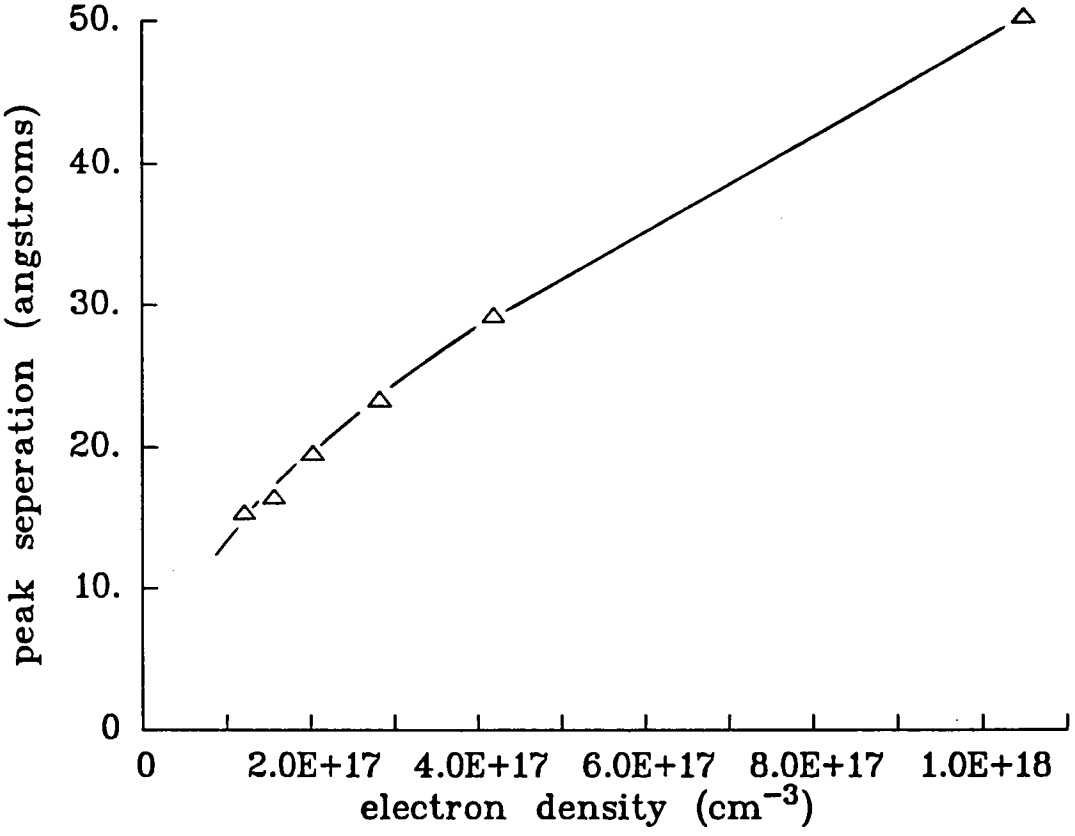

Figure 26: H_β peak separation at 810 torr

densities. The H_β lines that are emitted from regions with lower electron density have narrower line widths, and, therefore, less spectral separation of the red and blue peaks. This reduction in line width will tend to fill in the central portion of the overall profile and will result in a reduction in the peak separation of the overall profile. On this basis we would expect to see a reduction in the value of the constant a in Eq. 10 for a spatially inhomogeneous plasma.

7 TWO DIMENSIONAL EXPERIMENT

In an attempt to resolve the spatial inhomogeneities of the plasma, a two dimensional experiment was done. This experiment was accomplished in essentially the same way as the previous experiments. There were, however, some notable changes and improvements. A more accurate gauge was put into the system to monitor the cell pressure. This new gauge has a precision of $\pm$ 0.2 torr. The laser pulse was passed through a 3X beam expander prior to being focused into the cell. The expanded beam gives a more defined focus, and, therefore, a more stable laser spark. The laser pulse energy was increased to approximate 230 mJ per pulse and the laser pulse width was decreased to 6 ns.

The two dimensional aspect of the experiment enters through the detector. A CCD (Charge Coupled Device) camera was attached to the J-Y spectrometer. The 512 X 512 CCD chip of the camera allows for two dimensional detection of the plasma emission, one dimension being the spectral dispersion of the spectrometer, and the other dimension is the spectrometer slit.

The gas cell was rotated 90 degrees so that the laser pulse direction of propagation was parallel to the spectrometer slit. The resulting plasma was imaged one-to-one onto the spectrometer slit. The cell pressure for this experiment was 900 torr. The "length" of the laser spark was approximately 5 mm. The dimensions of the square CCD chip are 1 cm by 1 cm.

The spectrometer was centered on the H_α line and data were recorded in 6 ns

steps using a 6 ns gate out to a delay of 66 ns. Additional data points were acquired at delays of 96 ns, 200 ns and 300 ns using the 6 ns gate. Four time delays were recorded using a 20 ns gate: 500 ns, 750 ns, 1 μs and 1.5 μs. Two final data points were recorded at 2 μs and 3 μs using a 50 ns and 100 ns gate, respectively. The spectrometer slit was adjusted to 50 μm, which corresponds to a slit function FWHM of 0.6 Å and is negligible for most time delays. The trigger jitter of the gate delay is less than 2 ns.

Two dimensional H_α profiles are shown in Figs. 27 – 35. The laser propagation direction is in the positive x-direction, which corresponds to the vertical dimension of the CCD chip. The plots show a 5 mm portion of this vertical dimension.

There are several interesting aspects of these plots. Initially, the breakdown is most intense at the 3 mm point on the x-axis as is shown in Fig. 27. A time delay of zero means that we record the plasma emission with the detector gate centered on the laser pulse. Six nanoseconds later, Fig. 28, the initial peak moves forward and a second peak begins to emerge on the back side of the plasma. As the plasma expands the difference in the intensity between the two peaks decreases, see Figs. 29 and 30. The intensity minimum between the two peaks has a broader line width and therefore a higher electron number density. At 96 ns, Fig. 31, the two maxima are equal with small intensity variations in between. As the plasma decays further, the intensity maximum shifts to the back as Figs. 32 – 34 show. Finally, at 3 μs, there is only one peak, see Fig. 35. The position of this peak corresponds to the location of

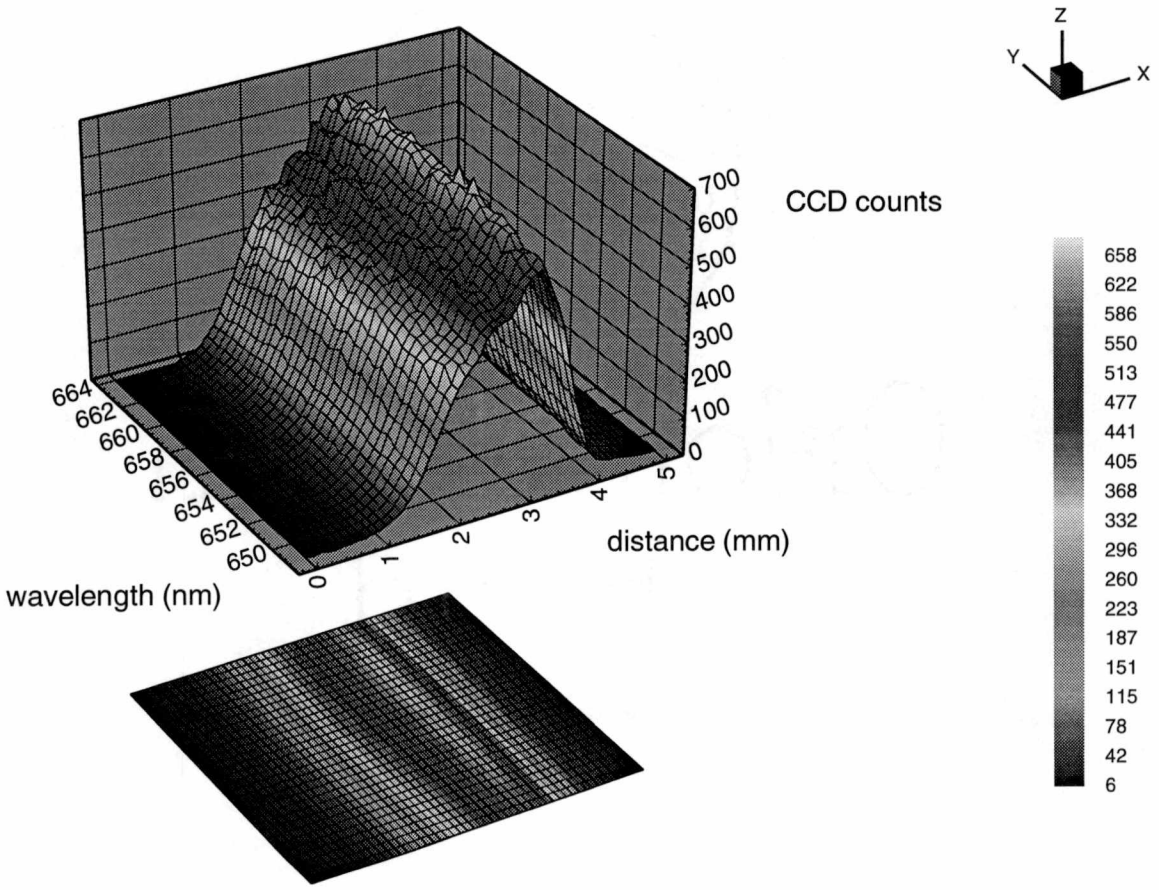

Figure 27: Two dimensional H_α profiles at zero time delay

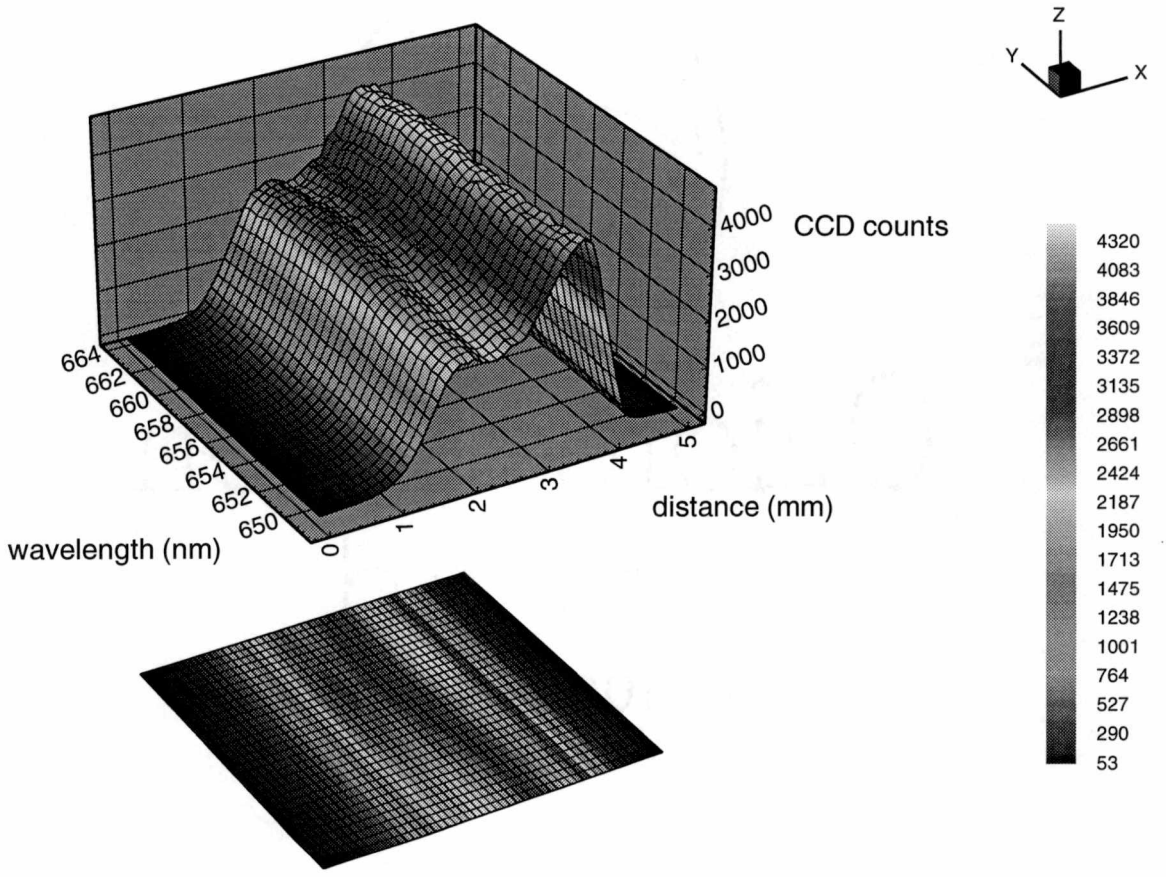

Figure 28: Two dimensional H_α profiles at 6 ns time delay

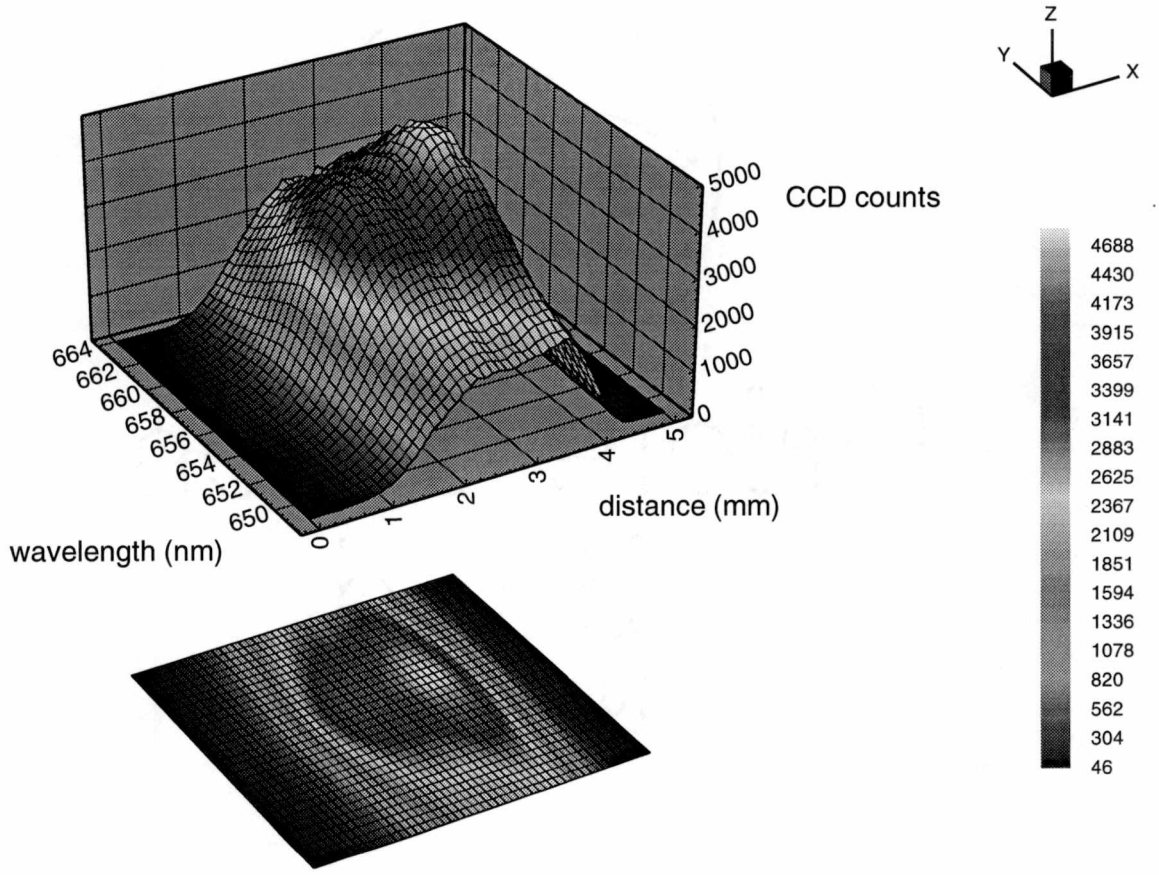

Figure 29: Two dimensional H_α profiles at 24 ns time delay

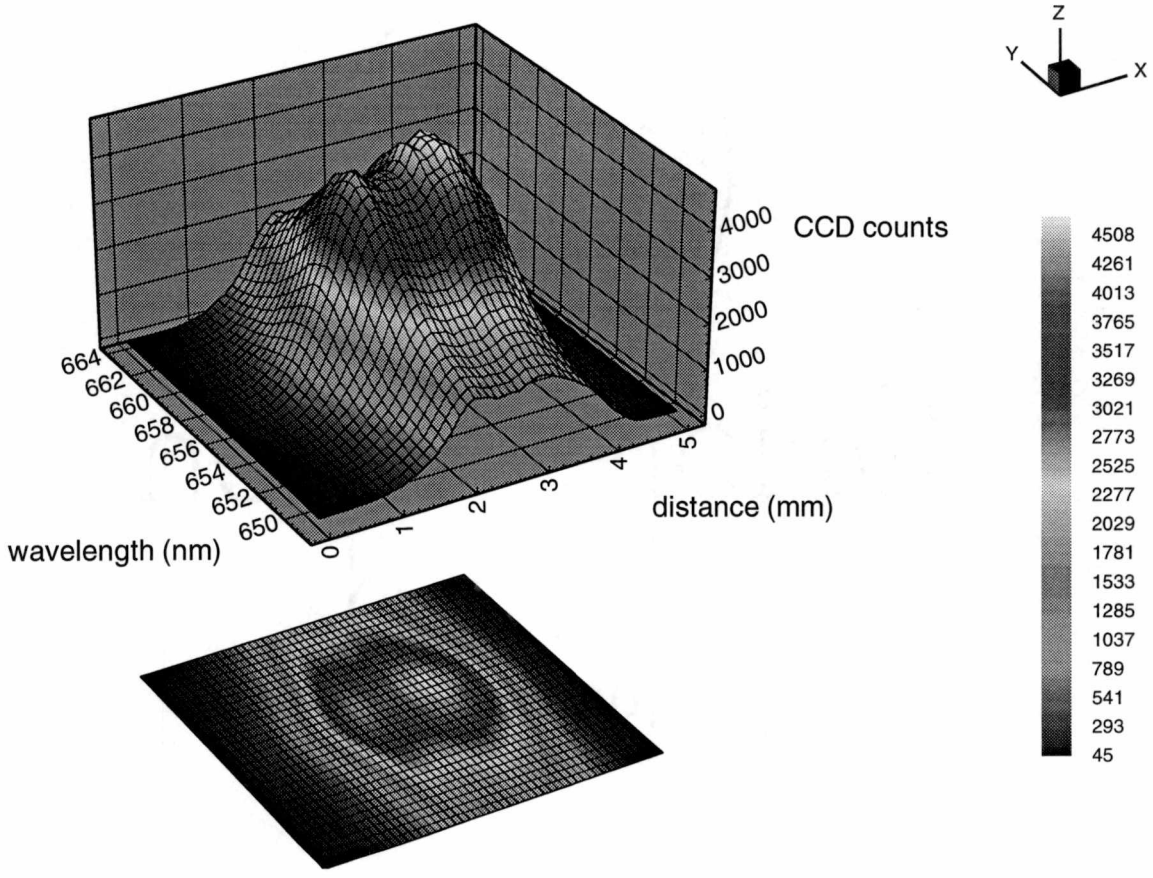

Figure 30: Two dimensional H_α profiles at 42 ns time delay

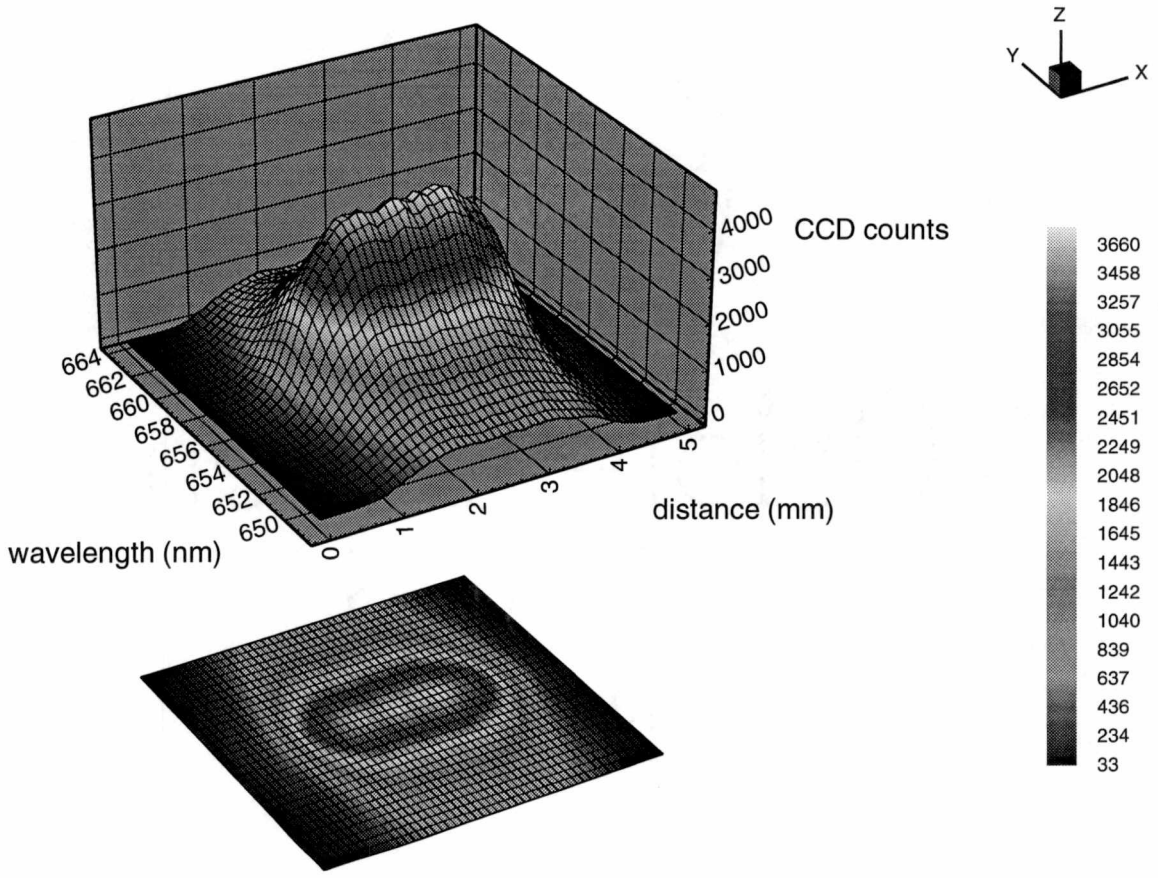

Figure 31: Two dimensional H_α profiles at 96 ns time delay

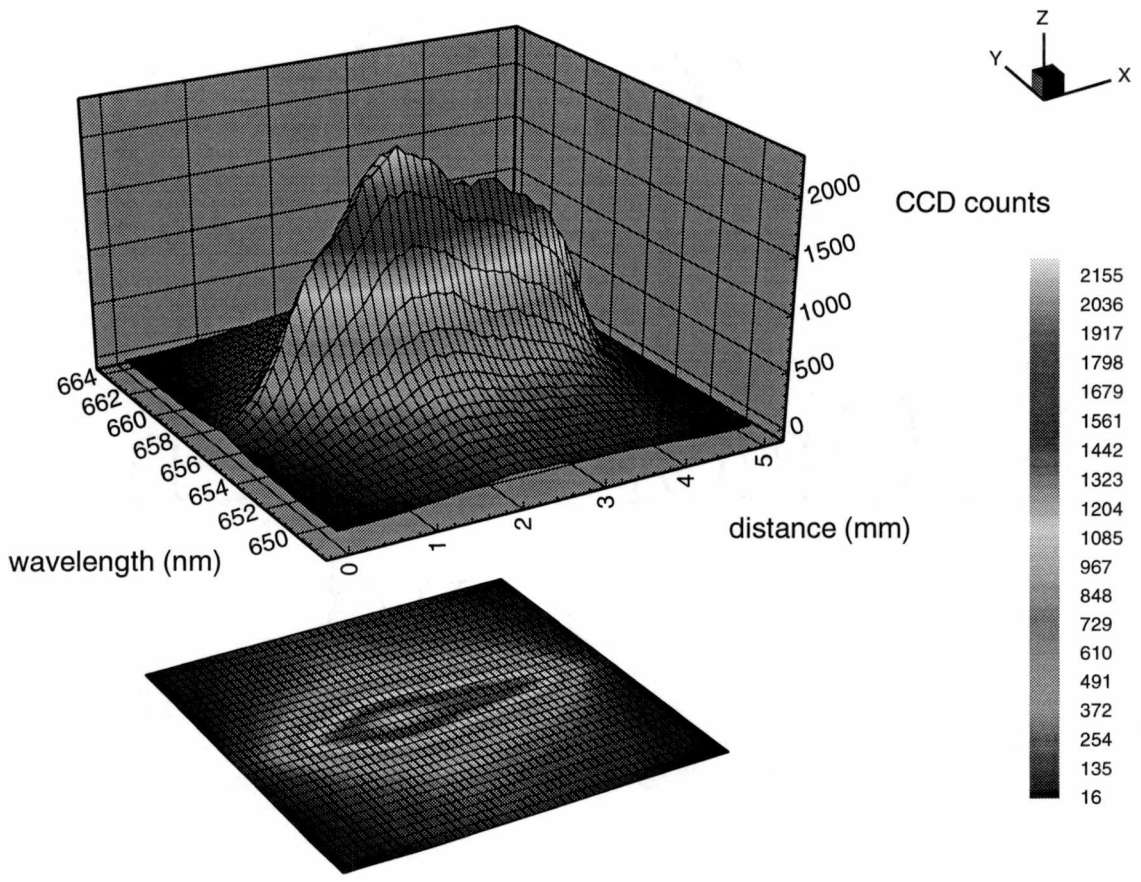

Figure 32: Two dimensional H_α profiles at 300 ns time delay

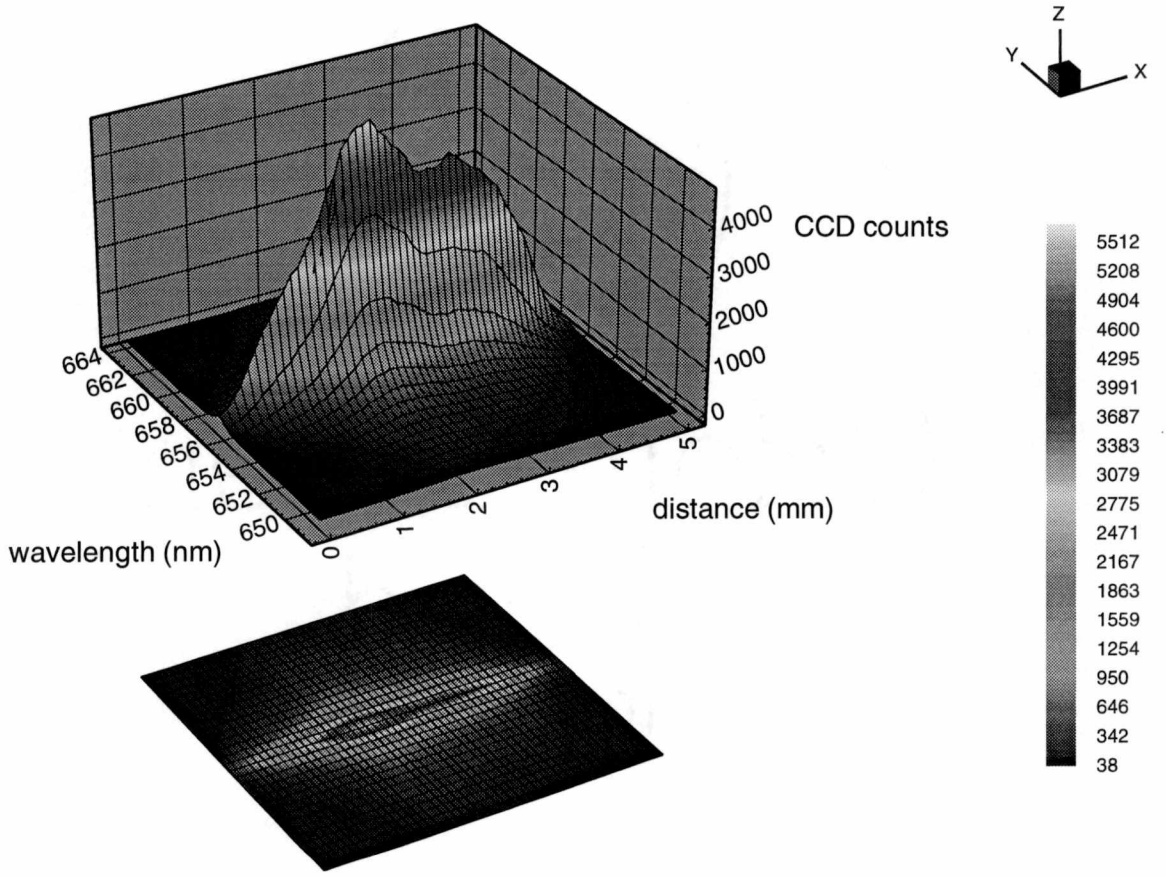

Figure 33: Two dimensional H_α profiles at 750 ns time delay

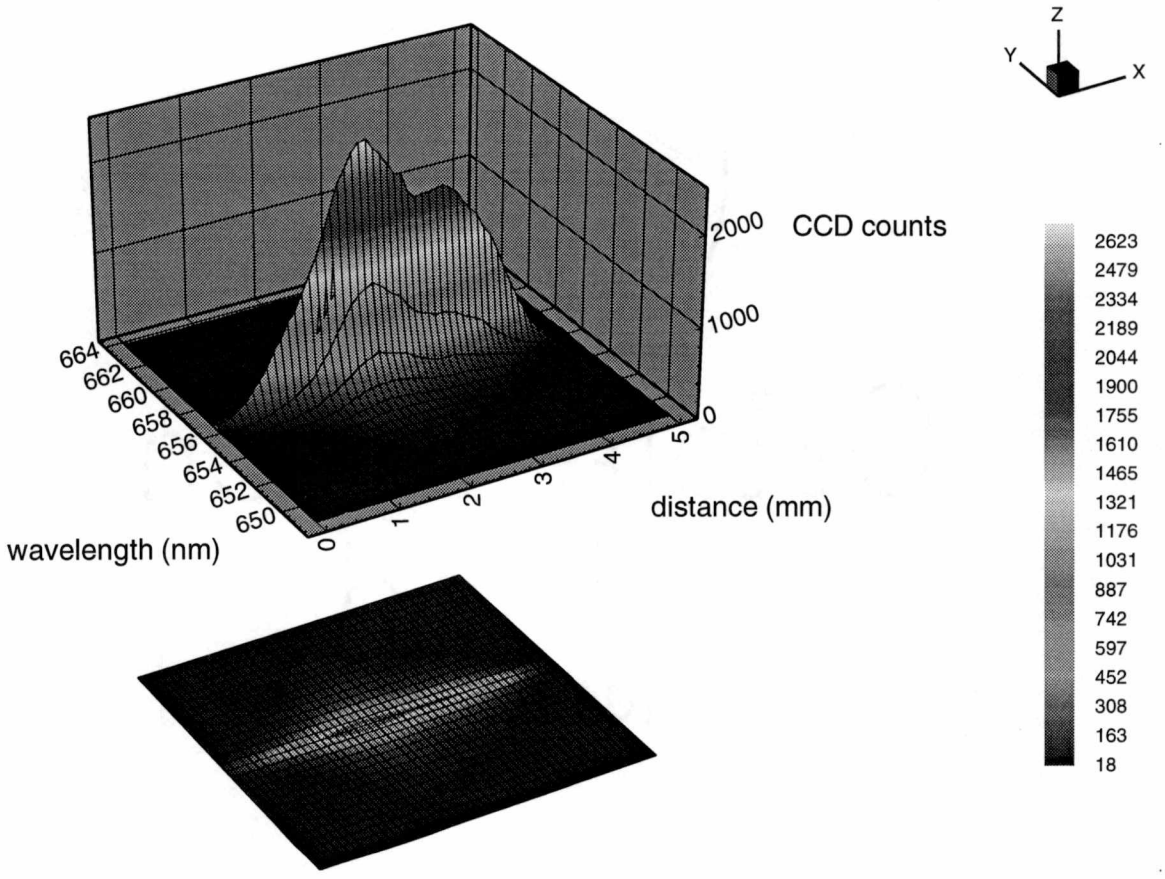

Figure 34: Two dimensional H_α profiles at 1.5 μs time delay

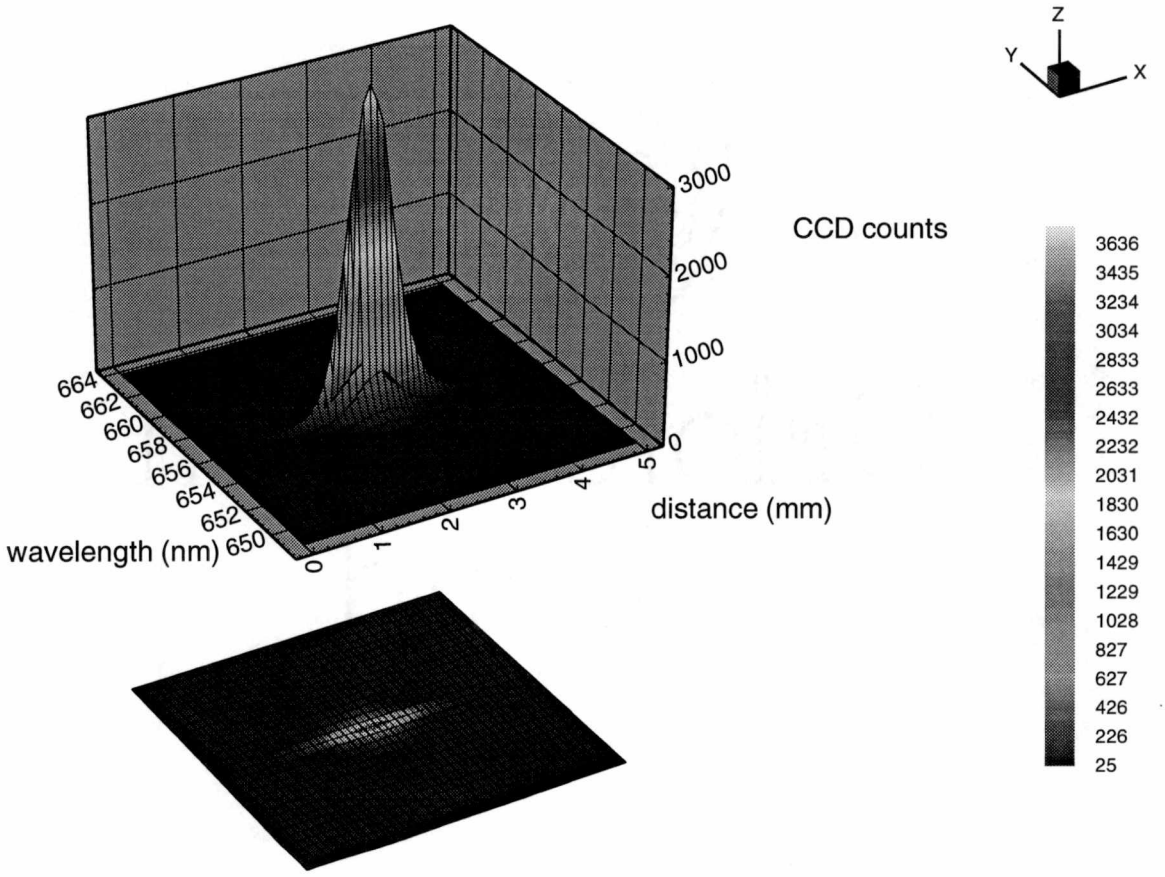

Figure 35: Two dimensional H_α profiles at 3.0 μs time delay

the minimum between the two peaks seen at earlier times. Note also that the position of maximum intensity of the H_α line is shifted by various amounts along the length of the laser spark, and that the shifts are also time dependent.

These figures show clearly that the laser-induced plasma is in a constant state of temporal and spatial change. If we were to monitor a vertical slice of the plasma across its shorter dimension, we expect to see regions of high or low electron temperature or density move by. Thus, we expect to see increases, decreases, or apparent inconsistencies in these parameters at some point in time in the plasma decay, depending on which portion of the laser spark was imaged onto the spectrometer slit.

Preliminary analysis, using H_α full profile fits, shows that the electron density across the length of the laser spark is not uniform. It is not surprising that the electron density is lower on the ends of the plasma, but the analysis shows that there also exist density variations in the central portion of the plasma.

This experiment shows that we must be cautious in the interpretation of the data sets recorded with the original experimental arrangement where the spectrometer slit is oriented perpendicular to the laser spark. The spatial variation of electron density and temperature across the plasma, and movement thereof, coupled with the uncertainty of which portion of the plasma is being observed could easily introduce differences in the results determined from different experiments.

8 DISCUSSION AND CONCLUSIONS

This thesis has presented the temporal evolution of electron number density and electron temperature of a laser-induced plasma in hydrogen gas. The electron temperatures were inferred from Boltzmann plots of the hydrogen Balmer series, and electron densities were inferred from Stark broadened H_α and H_β emission lines.

It has been found that the Boltzmann plots can be used on the Balmer series except at very early times in the plasma decay. This limitation is due to the extreme broadening of the Balmer lines at high electron number densities. In effect, we were able to use only two line Boltzmann plots for electron number densities greater than $\sim 1 \times 10^{18}$ cm^{-3}. For electron densities greater than $\sim 3 \times 10^{18}$ cm^{-3} an alternative method will have to be used, such as line-to-continuum ratios or Boltzmann plots of some multielectron atom introduced into the gas sample in small amounts.

Electron number densities have been determined using two methods. One consists of fitting theoretical profiles to experimental profiles. The other consists of measuring the full widths at half maximum of the experimental profiles. Both methods yield compatible results.

The H_α profiles can readily be used for electron density determination. The full profile fit appears to be the better method for H_α lines at high electron number densities or where the experimental profiles are incomplete. It is anticipated that for electron number densities much higher than 1×10^{19} cm^{-3} use of even the H_α line will be difficult.

The effects of a pressure variation on the electron number density and electron temperature were examined briefly. It was noted that the observed electron density change was not what would be expected from the change in number density of the hydrogen molecules due to the change in pressure. The electron temperature appears to be approximately independent of the pressure over the pressure range presented herein.

Electron density inference from H_β peak separation does not appear to be useful for our experimental conditions. The results that we obtained differ significantly from published theoretical and experimental results.

The full profile fitting technique is to be applied to the two dimensional H_α profiles recorded across the length of the laser spark and will yield spatially and temporally resolved electron densities across the laser spark. This experiment demonstrates, clearly, the spatial variations that exist in the laser-induced plasma. Detailed experiments are recommended to resolve spatially the electron temperatures.

A comparison of electron density results using H_α and H_β line widths shows that the results are consistent at early times but differ at later times. Further two dimensionally resolved experiments are recommended to address the differences between the number densities measured from the H_α and H_β profiles.

The Boltzmann plot and H_α experimental results were presented at the 1993 Optical Society of America conference [17] and will be submitted for publication in early 1994. The spatially resolved study of the laser-induced breakdown is scheduled

for presentation at the Laser Applications to Chemical Analysis Topical Meeting in March 1994 [18].

REFERENCES

References

[1] J. Stricker and J. G. Parker. "Experimental Investigation of Electrical Breakdown in Nitrogen and Oxygen Induced by Focused Laser Radiation at 1.064μ". *J. Appl. Phys.*, 53(2):851–855, 1982.

[2] J. O. Hornkohl, C. Parigger, and J. W. L. Lewis. "Temperature Measurements from CN Spectra in a Laser-Induced Plasma". *JQSRT*, 46(5):405–411, 1991.

[3] P. D. Maker, R. W. Terhune, and C. M. Savage. "Optical Third Harmonic Generation". In *III Int. Conf. on Quant. Electronics*, Paris, 1963.

[4] H. Haken and H. C. Wolf. *The Physics of Atoms and Quanta.* Springer-Verlag, New York, Berlin, and Heidelberg, 1993.

[5] J. B. Simeonsson and A. W. Miziolek. "Time-Resolved Emission Studies of ArF-Laser-Produced Microplasmas". *Appl. Opt.*, 32(6):939–947, 1993.

[6] P. Blau, I. Smilanski, and S. Rosenwaks. "Simultaneous Time-Averaged Measurements of Gas Temperature and Electron Density in a Copper-Vapor Laser Using Hydrogen Emission Spectroscopy". *J. Appl. Phys.*, 72(3):849–854, 1992.

[7] J. Ashkenazy, R. Kipper, and M. Caner. "Spectroscopic Measurements of Electron Density of Capillary Plasma Based on Stark Broadening of Hydrogen Lines". *Phys. Rev. A*, 43(10):5568–5574, 1991.

[8] J. H. Eickmans, W. F. Hsieh, and R. K. Chang. "Plasma Spectroscopy of H, Li, and Na in Plumes Resulting from Laser-Induced Droplet Explosion". *Appl. Opt.*, 26(11):3721–3725, 1987.

[9] V. Helbig and K-P Nick. "Investigation of the Stark Broadening of Balmer Beta". *J. Phys. B*, 14:3573–3583, 1981.

[10] D. E. Kelleher, N. Kongevic, and W. L. Wiese. "Test for Ion Dynamic Dependence of Plasma Red Shifts in Neutral Hydrogen". *Phys. Rev. A*, 20(3):1195–1196, 1979.

[11] H. R. Griem. *Spectral Line Broadening by Plasmas.* Academic Press, Inc., New York and London, 1974.

[12] D. H. Oza, R. L. Greene, and D. E. Kelleher. "Collisional Broadening of the Balmer-α Transition of H and He^+ in Plasmas". *Phys. Rev. A*, 37(2):531–536, 1988.

[13] W. L. Wiese D. E. Kelleher and D. R. Paquette. "Detailed Study of the Stark Broadening of Balmer Lines in a High-Density Plasma". *Phys. Rev. A*, 6(3):1132–1153, 1972.

[14] M. M. Litvak and D. F. Edwards. "Spectroscopic Studies of Laser-Produced Hydrogen Plasma". *IEEE J. Quant. Electron.*, QE-2(9):486–492, 1966.

[15] T. P. Evtushenko, A. N. Zaidel', G. V. Ostrovskaya, and T. Ya. Chelidze. "Spectroscopic Studies of a Laser Spark. I. Laser Spark in Helium ". *Sov. Phys. – Tech. Phys.*, 11(8):1126–1130, 1967.

[16] J. Uhlenbusch and W. Viöl. "H_β-Line Profile Measurements in Optical Discharges". *JQSRT*, 44(1):47–56, 1990.

[17] C. Parigger, D. H. Plemmons, and J. W. L. Lewis. "Electron Number Density and Temperature Measurement in a Transient Hydrogen Plasma". Optical Society of America – Annual Meeting. Toronto, Canada, 1993.

[18] C. Parigger, D. H. Plemmons, and J. W. L. Lewis. "Spatially and Temporally Resolved Electron Number Densities in a Decaying Laser-Induced Hydrogen Plasma". Optical Society of America – Laser Applications to Chemical Analysis Topical Meeting. Jackson Hole, Wyoming, 1994.

[19] H. R. Griem. *Plasma Spectroscopy.* McGraw-Hill, New York, 1964.

[20] A. P. Thorne. *Spectrophysics.* Chapman and Hall, New York, 1988.

[21] H. R. Griem. "Shifts of Hydrogen Lines from Electron Collisions in Dense Plasmas". *Phys. Rev. A*, 28(3):1596–1601, 1983.

[22] J. Siedel. "effects of ion motion on hydrogen stark profiles". *Z. Naturf.*, 32a:1207–1214, 1977.

[23] L. P. Kudrin and G. V. Sholin. "Asymmetry of Spectral Lines of Hydrogen in Plasma". *Soviet Phys. - Dok.*, 7(11):1015–1017, 1963.

[24] A. E. Siegman. *Lasers.* University Science Books, California, 1986.

APPENDIXES

A Description of the Laser Spark

For reference we give here a brief description of the laser spark. The following calculations are based on a Gaussian laser beam. The diameter of the beam is taken to be the distance across the Gaussian intensity profile at the point where the intensity drops to $1/e$ of the peak intensity. A Gaussian beam is realized when the laser is operated in the TEM_{00} cavity mode. The Nd:YAG laser used in this experiment has multi-mode output, and the resulting output pulse is not Gaussian. Therefore we expect the following calculations to represent only the limiting case.

A Gaussian beam with wavelength λ and beam diameter d can be focused to a minimum diameter, D, given by [24]

$$D \approx 2\frac{\lambda f}{d} \Rightarrow \frac{D}{\lambda} \approx 2\frac{f}{d} \tag{11}$$

where f is the focal length of the lens. The output pulse of the Nd:YAG laser has a beam diameter of approximately 5 mm. Thus, for 1.064 μm radiation focused with a 10 cm lens the spot size is approximately 43 μm. For a 150 mJ, 7.5 ns, laser pulse, this gives a power density of approximately 1400 GW/cm^2. This power density is more than ten times larger than the nanosecond breakdown threshold of hydrogen gas for 1.064 μm radiation.

The Rayleigh range of the focus laser pulse is defined as the distance away from the focal spot where the beam diameter has increased to $\sqrt{2}D$ and is given by the

expression

$$Z_R \approx \frac{\pi}{4}\frac{D^2}{\lambda} \Rightarrow \frac{Z_R}{\lambda} \approx \frac{\pi}{4}(\frac{D}{\lambda})^2. \tag{12}$$

This gives a Rayleigh range of approximately 1.3 mm for the parameters given above. The focal volume of the focused laser pulse is given by

$$V_f \approx \pi(\frac{D}{2})^2(2Z_R) \Rightarrow \frac{V_f}{\lambda^3} \approx \frac{\pi}{2}(\frac{D}{\lambda})^2(\frac{Z_R}{\lambda}), \tag{13}$$

which gives, for 1.064 μm radiation, $V_f \approx 4 \times 10^{-6}$ cm^{-3}. Thus, the power density is high enough to induce breakdown over a significant distance.

We know from previous experiments that the focal diameter of a typical Nd:YAG laser pulse is approximately 80 μm. Using this value for the spot size, Eq. 12 gives $Z_R \approx 5$ mm, and Eq. 13 gives $V_f \approx 5 \times 10^{-5}$ cm^{-3}. The power density for the 80 μm spot size is approximately 400 GW/cm^2, which is approximately four times the breakdown threshold.

For the hydrogen plasma the plasma frequency is

$$\omega_p = (\frac{e^2 N_e}{\epsilon_0{}^2 m_e})^{1/2}. \tag{14}$$

The Debye shielding radius is

$$r_D = (\frac{\epsilon_0 k_B T}{2e^2 N_e})^{1/2}. \tag{15}$$

For a temperature of 10^4 K and electron density of 10^{18} cm^{-3}, eqs. 14 and 15 yield $\omega_p = 5.6 \times 10^{13}$ s^{-1} and $r_D = 6.9$ nm.

Figure 36 – 38 show shadowgraph images of shock waves associated with breakdown pulses for delays of 13, 60 and 135 ns. These images were acquired for breakdown

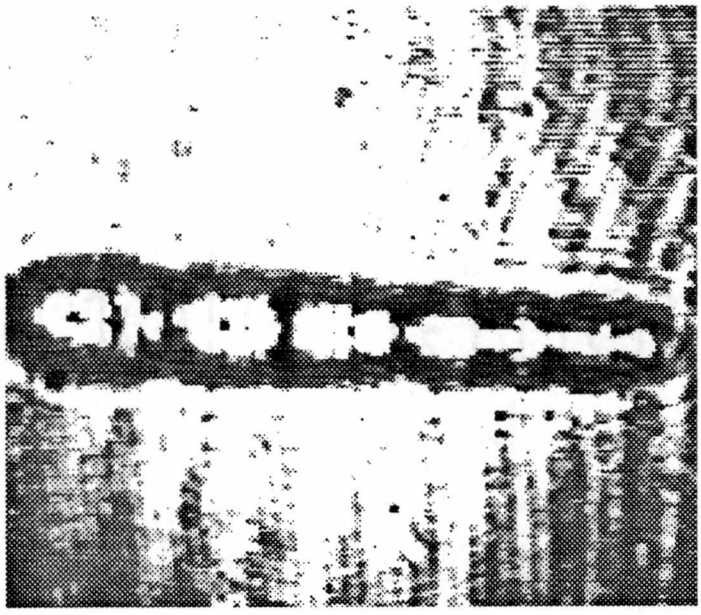

Figure 36: Shadowgraph image of shockwave: backlight delay = 13 ns

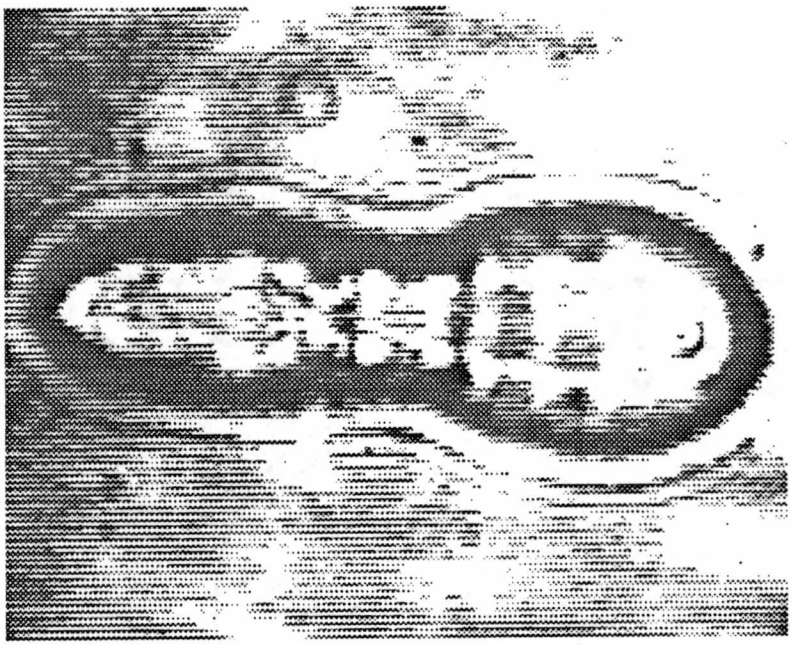

Figure 37: Shadowgraph image of shockwave: backlight delay = 60 ns

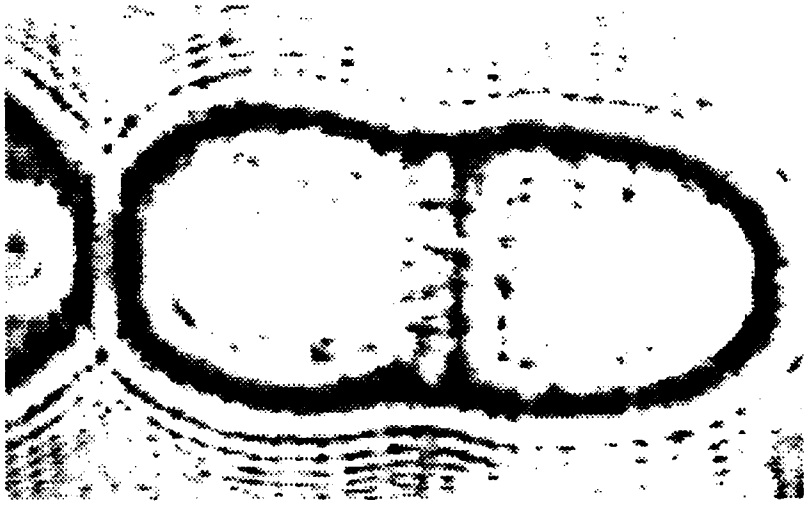

Figure 38: Shadowgraph image of shockwave: backlight delay = 135 ns

in nitrogen gas, with 100 mJ of energy per laser pulse, but are typical for breakdown in hydrogen gas. The length of the shockwave is approximately 6 mm in the 13 ns image, and the other two images are shown to the same scale.

These images were obtained by passing a portion of the 1.064 μm Nd:YAG laser pulse through a frequency doubler and using the frequency doubled pulse as a backlight. The backlight pulse was optically delayed using a series of mirrors and directed through the gas cell perpendicular to the direction of propagation of the breakdown pulse. The plasma emission region is smaller than the extent of the shockwave, but, is approximately the size of the 13 ns image shown in Fig. 36. This shadowgraph illustrates the point of a long, thin breakdown region. Notice also the structure within the shockwave. This structure is indicative of hot spots in the plasma. The laser pulse appears to have initiated breakdown at several different locations along its path of propagation. This effect is most likely due to self-focusing effects of the plasma. These hot spots are a source for the inhomogeneities that exists in the plasma. The vertical structure in the images is where individual shock waves have collided as they expand.

B Deconvolution of the Slit Function

For the Jarrell-Ash quarter-meter spectrometer with the 1800 g/mm grating we have a maximum resolution of 0.55 Å as dictated by the physical dimension of individual photodiodes in the array and the reciprocal linear dispersion of the grating. With the entrance slit set to 200μm, the spectral resolution is approximately 2.5 Å. This resolution is measured from the FWHM of a hydrogen calibration lamp. The full profile of the H_α line is taken as the slit function of the instrument.

It was pointed out in Chapter 3 that a Stark profile is predominantly Lorentzian. The slit function is approximately Gaussian. The convolution of a Gaussian profile with a Lorentzian profile yields a Voigt profile. The FWHM of a Voigt profile is not the sum of the Doppler FWHM and the Lorentzian FWHM. To determine the contribution of the slit function to the FWHM of the Stark broadened H_α line we need to deconvolve the slit contribution from the experimental profile. This task is more readily accomplished in reverse. That is, we convolve the slit function with theoretical profiles and use the result to determine the contribution of the slit to the experimental profile.

Griem's theoretical profiles at 10,000 K and various electron densities are convolved with the slit function. The actual FWHM is then taken as the difference between the FWHM of the convolved profile and that of the theoretical profile. As is expected, the contribution of the slit to the actual FWHM is not simply an additive effect. The convolution results are listed in Table 9. The theoretical and convolved

Table 9: Convolution of H_α theoretical profiles with spectrometer slit function

theoretical FWHM (Å)	$(N_e)_{theory}$ (cm^{-3})	convolved FWHM (Å)	$(N_e)_{convolved}$ (cm^{-3})	$\Delta\lambda_{1/2}$ (Å)	ΔN_e (cm^{-3})
1.528	1.0×10^{16}	4.419	3.36×10^{16}	2.891	2.36×10^{16}
2.894	2.0×10^{16}	5.572	4.53×10^{16}	2.678	2.53×10^{16}
4.038	3.0×10^{16}	6.582	5.65×10^{16}	2.544	2.65×10^{16}
5.061	4.0×10^{16}	7.510	6.75×10^{16}	2.449	2.75×10^{16}
6.000	5.0×10^{16}	8.380	7.84×10^{16}	2.380	2.84×10^{16}
6.880	6.0×10^{16}	9.203	8.92×10^{16}	2.323	2.92×10^{16}
7.711	7.0×10^{16}	9.988	9.99×10^{16}	2.277	2.99×10^{16}
8.503	8.0×10^{16}	10.74	1.10×10^{17}	2.237	3.00×10^{16}
9.262	9.0×10^{16}	11.47	1.19×10^{17}	2.208	2.90×10^{16}
9.994	1.0×10^{17}	12.17	1.29×10^{17}	2.176	2.90×10^{16}
17.00	2.0×10^{17}	18.94	2.32×10^{17}	1.940	3.20×10^{16}
28.11	4.0×10^{17}	29.95	4.37×10^{17}	1.840	3.70×10^{16}
37.43	6.0×10^{17}	39.33	6.44×10^{17}	1.900	4.40×10^{16}
45.75	8.0×10^{17}	47.76	8.51×10^{17}	2.009	5.10×10^{16}
53.39	1.0×10^{18}	55.57		2.180	

FWHM's are plotted in Fig. 39 and the differences are shown in Fig. 40.

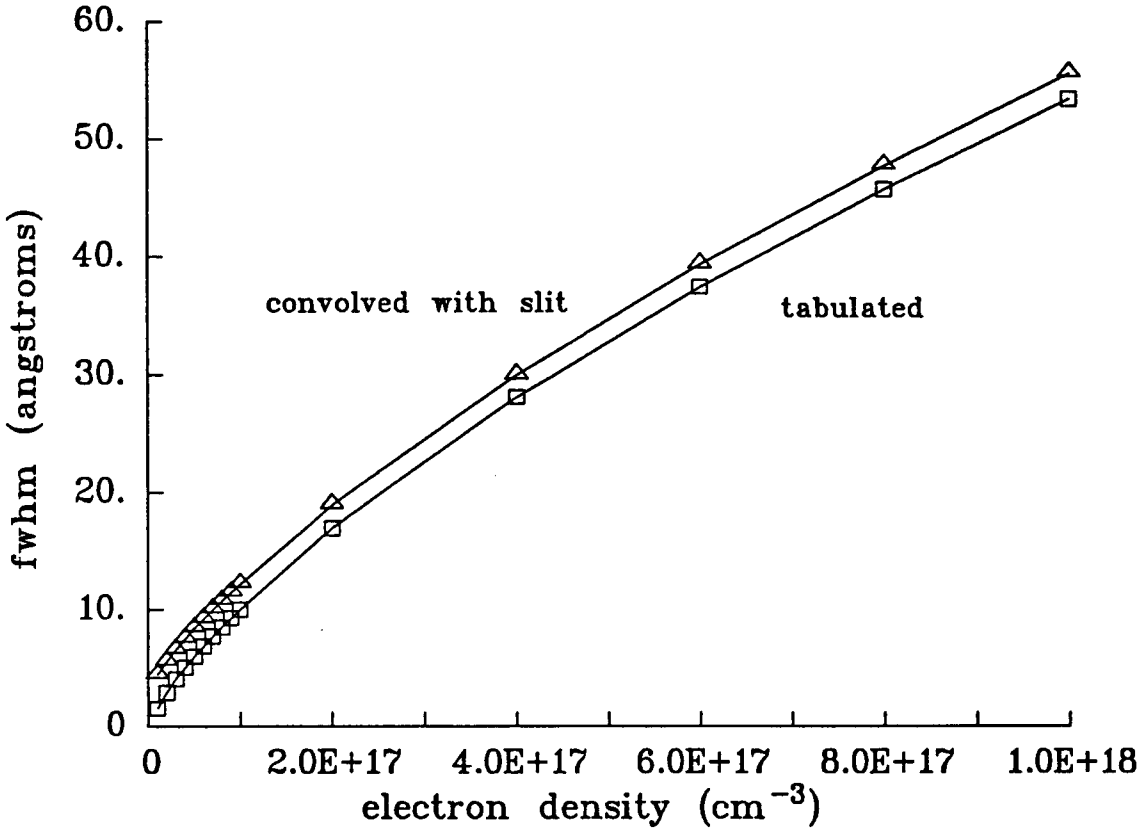

Figure 39: Tabulated and convolved FWHM's

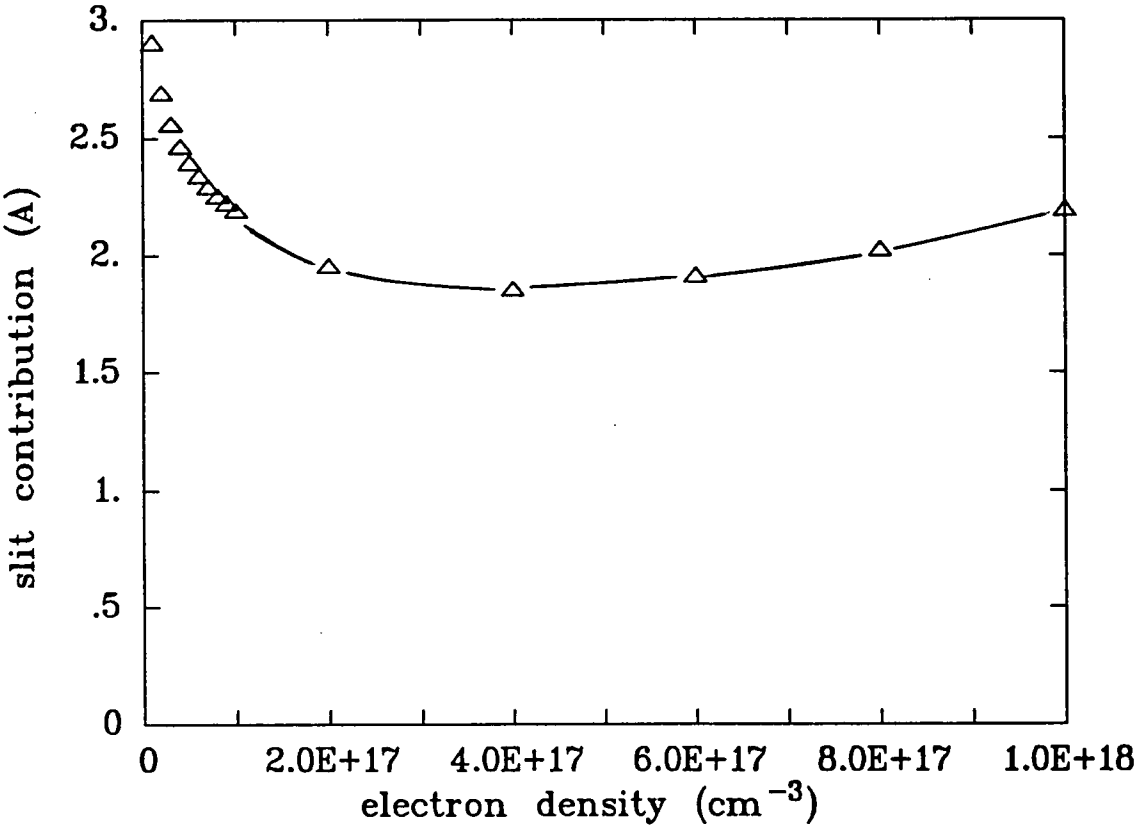

Figure 40: Convolved FWHM's minus tabulated FWHM's

VITA

David Plemmons was born in Memphis Tennessee on April 26, 1962. He studied Civil Engineering for two years at the University of Tennessee, Martin. In January 1984 he transferred to Middle Tennessee State University and received a Bachelor's degree in Aerospace Maintenance Management in August 1986. After working for several years as an aircraft technician he reenrolled in Middle Tennessee State University, and, in December 1990, received Bachelor's degrees in Physics and Mathematics. He entered graduate school at the University of Tennessee Space Institute in January 1991 and earned a Master's degree in Physics in May 1994.